Composites Part B 224 (2021) 109148

Contents lists available at ScienceDirect

Composites Part B

journal homepage: www.elsevier.com/locate/composites

New experimental insights into magneto-mechanical rate dependences of magnetorheological elastomers

M.A. Moreno, J. Gonzalez-Rico, M.L. Lopez-Donaire, A. Arias, D. Garcia-Gonzalez *

Department of Continuum Mechanics and Structural Analysis, University Carlos III of Madrid, Avda. de la Universidad 30, 28911 Leganés, Madrid, Spain

ARTICLE INFO

Keywords:
Magneto-rheological elastomers (MREs)
Magneto-mechanical rheology
Multifunctional composites
Viscoelasticity
Smart materials
Experimental mechanics

ABSTRACT

Magnetorheological elastomers (MREs), consisting of an elastomeric matrix filled with magnetic particles, are one of the most promising multifunctional composites. The main advantage of these materials is their response to external magnetic fields by mechanically deforming and/or changing their magnetorheological properties. This multi-physical nature makes them ideal candidates for timely applications in soft robotics and bioengineering. Although several works have addressed the magneto-mechanical coupling in these composites from both experimental and modelling approaches, there is still a big gap of knowledge preventing the full understanding of their underlying physics. In this regard, there is no experimental work addressing a comprehensive magneto-mechanical characterisation combining different MRE configurations, mechanical deformation modes and magnetic conditions. Furthermore, the interplays of rate dependences into such magnetorheological behaviour still remain elusive. In this work, we provide an unprecedented experimental characterisation of a soft MRE considering more than 100 different experimental conditions involving more than 600 tests. The experiments include monotonous uniaxial compression at different deformation rates and magnetic conditions, magneto-mechanical DMA tests, relaxation tests, oscillatory shear tests at different deformation rates and magnetic conditions, magneto-mechanical shear frequency sweep tests, and novel magneto-mechanical experiments. The results obtained in this work provide full characterisation of soft MREs with a special focus on rate dependences, forming the basis to explain novel multifunctional mechanisms identified behind their coupled response. In addition, it opens the door to new constitutive and modelling approaches.

1. Introduction

Multifunctional materials are revolutionising the engineering fields due to the ability to modify their properties by applying an external stimulus. Among them, smart materials that respond to magnetic fields are of particular interest as they offer possibilities for remote and reversible stimulation. These are called magneto-active polymers (MAPs) or magneto-rheological (MR) materials. These structures count on dispersed magnetic fillers which are responsible of the magnetostrictive response (i.e., mechanical deformation to an applied magnetic field) [1–3]. Depending on the nature of the carrier matrix, a MR material can either be a fluid, a gel or an elastomer [4,5]. In 1948, Rabinow [6] introduced MR fluids. These, under the application of an external field, become non-newtonian fluids with a stiffness up to four orders larger [7]. Sedimentation and formation of aggregates, however, are issues of these composites [8,9]. MR gels have intermediate properties between MR fluids and elastomers, and have the magnetic particles and solvent molecules (e.g., water) embedded within a cross-linked polymer network (i.e., hydrogel). This microstructural configuration allows for particles' movement to form chain-like structures, while they retain the original configuration once the magnetic field disappears [10–12]. Regarding magneto-rheological elastomers (MREs), magnetic fillers remain at the positions they reach during the curing process (although extremely soft elastomeric matrices lead to very large changes in particles' distribution when subjected to a magnetic field). Their carrier matrix is a vulcanised polymeric network with higher stiffness than that of MR fluids and gels. Despite their ability to change their shape (i.e., tuning by deformation mode branching [13]), MREs have been mostly studied for their capacity to change their mechanical properties [14–16]. In addition, Xu et al. [17] introduced MR plastomers as materials with plastic properties at room temperature [18]. According to the purpose of this work, in the following, MREs are reviewed.

The carrier matrix of MREs can be made of different materials, e.g., silicone rubbers, vinyl rubbers (VR), polyurethanes (PU) or natural

* Corresponding author.
E-mail addresses: migmoren@ing.uc3m.es (M.A. Moreno), danigarc@ing.uc3m.es (D. Garcia-Gonzalez).

https://doi.org/10.1016/j.compositesb.2021.109148
Received 25 May 2021; Received in revised form 23 June 2021; Accepted 13 July 2021
Available online 18 July 2021

rubbers [19–22]. Regarding the manufacturing of MREs, the base phase and a cross-linking phase (sometimes with a catalyst) are put together and undergo the so-called curing process, which results in the cross-linked polymeric matrix. Depending on the amount of vulcaniser, the cross-linking degree of the matrix can be tuned [23–25]. Magnetic particles, which can be either soft or hard magnetic, are added to the raw mixture. Soft-magnetic particles (i.e., with low magnetic coercivity) are preferred when reversible property-changing effects of the composite are desired. However, hard-magnetic particles (i.e., with high magnetic coercivity) are used when shape-changing abilities are required. Additionally, some authors present novel approaches of hybrid MREs with mixed soft and hard magnetic fillers. In this way, Borin et al. [26] decouple the magnetic effect in passive state properties, for the pre-magnetised hard particles, and in active state properties controlled by an externally applied magnetic field. The distance between the particles, hence the intensity of the dipole–dipole interaction, can be tuned by modifying the particles concentration (see Ivaneyko et al. [27] work). Also, the stretch/contraction of the MRE in finite deformations changes the spacing between the fillers. In this regard, Garcia-Gonzalez et al. [28,29] predict the magnetic stress versus stretch for various microstructural space arrangements of the magnetic particles. Furthermore, if an external magnetic field is applied on the mixture during the curing process, the MRE acquires anisotropic properties with improved stiffness in the preferred direction of the particle chains. All in all, MREs with suitable properties for specific applications can be obtained by conveniently defining the manufacturing conditions.

Some exploitable areas of MREs are engineering, materials and biomedical sciences [30]. Common applications comprise soft robotics [31,32], mechanical damping systems [33–37], sandwich structures [38], tactile displays and sensors [39–42], microfluid transportation systems [43] and peristaltic pumps [44]. Some of these applications lay on the dynamic behaviour of MREs for certain excitation frequencies, e.g., low frequencies (below 100 Hz) are used when it comes to suspension applications for vehicles and biomedical applications [23,45], whereas frequencies in the order of kHz are excited in noise and vibration cancellation applications. Bioengineering applications of MRE are gaining popularity [46]. Drug delivery systems promise to locally treat pathologies with higher effectiveness and fewer side effects [47,48]. In this regard, Hu et al. [49] designed small-scale soft-bodied robots with multi-modal locomotion made of silicone elastomer with hard magnetic particles. These micro-robots, able to negotiate obstacles, would be suitable for cell manipulation, drug delivery, non-invasive surgery, etc. Moreover, MREs could be used as potential substrates for cell migration stimulation [23,50].

In order to design new applications of MREs, an excellent knowledge of their mechanical response and coupled governing magneto-mechanical phenomena is mandatory. To this end, experimental methods bring actual information about the macroscopic response of the composite subjected to external stimuli. The most common ones are [18]: compression/tensile tests, biaxial counterparts, simple shear test, fatigue test, dynamic mechanical analysis (DMA) and vibration analysis. Owing to the viscous nature of MREs, special attention on deformation and magnetic rates is required. For this reason, magneto-mechanical rheology is often used to characterise visco-elastic materials in multiple modes, i.e., shear, axial, temperature or magnetic modes. Oscillatory rheology has been widely used to determine the response of MREs when working in shear deformation [51–56]. Moreover, uniaxial compression experiments bring relevant information, as the material is deformed in the same direction of the applied magnetic field [57,58]. In the literature, however, there is not much work that synthesises multiple deformation modes and discusses the underlying mechanisms and interlinks between mechanical and magnetics phenomena. In addition, to the authors' knowledge there is no available work addressing the couplings between mechanical and magnetic rate dependences.

In this work, we provide a holistic framework for the rheological characterisation of magneto-rheological elastomers, considering more than 100 experimental conditions and combining different mechanical deformation modes and magnetic loading. The experimental campaign includes monotonous uniaxial compression tests at different deformation rates and magnetic conditions, magneto-mechanical DMA tests, relaxation tests, oscillatory shear tests at different deformation rates and magnetic conditions, magneto-mechanical shear frequency sweep tests, and novel magneto-mechanical experiments (see Fig. 1c for magneto-mechanical deformation modes). First, we present the full characterisation framework of extremely soft MREs. Far from just conveying the results, special focus has been put on producing detailed discussions about the underlying multifunctional phenomena. To this end, we have developed a discussion based on the quantitative results and with supplementary experiments about the magneto-mechanical coupling phenomena.

2. Materials and methods

2.1. Material and synthesis

For this study we have considered MREs composed of a soft elastomeric matrix and soft magnetic particles. A common matrix used in the literature is Sylgard 184 [23], but this elastomer presents high stiffness limiting the magnetostrictive response of the composite. To overcome this limitation, other authors have used softer elastomers, i.e., Eco-Flex silicone rubber [52,59,60]. With the aim of developing optimal MREs for bioengineering applications [24,61], the chosen elastomeric phase is Dowsil CY52-276 (DowSil, Midland, MI, USA) (PDMS), provided in two phases. Both phases get cross-linked by the so-called curing process as they are combined in a ratio of 1:1, according to the manufacturer indications. To avoid discrepancies in the raw material, the same batch is used to manufacture all the samples. Regarding the magnetic particles, these are soft SQ carbonyl iron powder (CIP) (BASF, Germany), obtained from thermal decomposition of iron pentacarbonyl and with a mean diameter of 3.9–5 μm. These particles present soft-magnetisation characteristics that make them highly suitable for applications where the tuning of the mechanical properties of the structure is desired. The size of the particles, contrary to smaller nanometric magnetic fillers, enables for sufficient magnetisation and enhances the magnetorheological response of the MRE.

For the selection of PDMS-magnetic particles' ratios used in this work, we have considered the following two limitations: (i) the mixture can become too viscous to be processed, up to 40 vol.% according to Lokander [62], and (ii) the existence of a percolation threshold, which is related to the capacity of the particles to move along the carrier matrix and occurs above 20 vol.% [58]. Therefore, four different samples have been considered consisting of PDMS with phases mass ratio 1:1 and particles' volume fraction (ϕ) of 0, 0.1, 0.2 and 0.3. To manufacture the samples, we have followed the process depicted in Fig. 1a.

2.2. Experimental setup

The rising interest in MREs requires the use of experimental characterisation techniques that combine traditional rheology with the application of external magnetic fields to evaluate the magneto-mechanical properties of the material [63]. The magneto-rheological mechanism is based on the differences in magnetic permeability between the continuous phase (carrier matrix) and the dispersed phase (magnetic particles). The magnetic particles get magnetised when subjected to a magnetic field. Consequently, each particle becomes a magnetic dipole leading to interaction forces with the remaining particles and the external magnetic field. Opposed to these forces, the polymeric matrix acts as a deformation barrier transmitting the internal stresses within the composite. The consequence is a macroscopic deformation or, in case of being confined, an increase in material stiffness (the so-called magneto-rheological effect) [18]. The magnitude of such deformation or change

in the material properties will depend on the particles' volume fraction, size, and their magnetic properties (i.e., relative permeability, magnetic saturation). In addition, the spatial arrangement of the particles will determine the intensity and orientation of the interaction forces between them (i.e., isotropic and anisotropic structures).

In this work, a TA HR-20 rheometer with Magneto-Rheology Accessory from Waters TA Q600 (TA instrument, New Castle, DE, USA) is used, see Fig. 1. The magnetic field is applied by a magneto-rheological accessory that sets a magnetic field in the axial direction to the sample. Note that the device is equipped with a close loop system to control the applied magnetic field measuring it in the vicinity of the sample. To prevent temperature variations due to Joule effect from the coils and keep a constant temperature, a cooling system is integrated with the device to set a constant temperature within the sample of 25 ^{o}C. An important remark is that, to ensure homogeneous fields, an upper yoke is added. This limits the sample size to 1 mm height and 20 mm diameter. Note that the parallel plates are made of low magnetic permeability stainless steel. In addition, the device has a magnetic axial bearing that allows to carry out oscillatory tests under both shear load and axial loading conditions in the longitudinal axis.

3. Magneto-mechanical characterisation under uniaxial loading

An important consideration about these tests relates to barrelling effect, widely reported when deforming cylindrical samples [64,65]. In this regard, the adhesion along the sample-machine interface gives rise to frictional contact that may not correspond to free-slip boundary conditions. Therefore, radial shear stress components should be considered on the sample-plate interfaces, leading to higher macroscopic stiffness of the structure. For this reason, and to ensure free displacement of both upper and lower surfaces, we have applied a lubricant coating on the sample (on both upper and lower surfaces) before performing every test. In this way, it is guaranteed that the lubrication conditions are repetitive for all the tests and radial shear stresses on the interfaces can be neglected.

3.1. Monotonous uniaxial compression tests

These experiments are conducted to a final strain of 45% and at three strain rates $\dot{\epsilon} = \{0.03, 0.3, 0.7\}$ s^{-1}, for each particles' volume fraction $\phi = \{0, 0.1, 0.2, 0.3\}$. We performed six repetitions for each experimental condition to ensure repeatability. These results are collected in Fig. 2 by means of engineering stress versus engineering strain showing average curves and experimental dispersion.

The average curves in each sub-figure correspond to different magnetic particle's volume fractions for a same strain rate. In addition, scatter areas are drawn as an intuitive way to define the space that comprises the raw experimental data, for the same test conditions. These results show clear trends in the mechanical response of the MREs. For every condition, the stress–strain curve presents a quasi-linear region at small displacements that becomes non-linear for larger strains. In addition, the stiffness of the samples always increases with the amount of magnetic particles, regardless which deformation rate is considered. Such an increase is explained by the much higher stiffness of the particles and their contribution hindering the polymer chains movement within the carrier matrix. Special attention is given to the stiffening from $\phi = 0.2$ to $\phi = 0.3$, for which the difference is notably smaller than the one that occurs as the magnetic particle's volume fraction increases from 0 to 0.2. This observation is explained by the percolation threshold that, from $\phi = 0.2$, promotes the formation of clusters and other sorts of aggregates. This feature would justify the decrease in the stiffening effect of the magnetic particles at high volume fractions [58]. Furthermore, viscoelastic effects are observed by means of strain rate dependency. In this regard, higher compression rates result in higher MRE stiffness. This rate dependency is directly related to stress states owing to viscous dissipation phenomena, which is deeper investigated in the following Sections 3.2 and 3.3 .

3.2. Relaxation tests

Relaxation tests are conducted to examine viscous mechanisms by applying a fixed strain and monitoring the evolution of the stress state along time. The initial deformation step is applied by setting a fast strain rate of 0.7 s^{-1} (maximum value allowed by the experimental system), which is followed by a relaxation time at constant strain of 90 s. These results, for the different MREs tested, are presented in terms of engineering stress versus engineering strain curves for strains of 40% and 25%, see Fig. 3. The analysis of these tests is performed by means of characteristic relaxation times. These are defined as the time that an exponentially decreasing variable takes to accomplish a 63.21% of the stress relaxation for infinite time (i.e., exponential decay). Overall, these results show different tendencies. A clear increase in the characteristic relaxation time is observed when increasing the particles' content. Thus, relaxation times range from around 1 s, for the case of PDMS without magnetic particles, to 6.5 s, for the case of $\phi = 0.3$ (see further details in Table 1). In this regard, the inclusions in the carrier matrix hinder the mobility of the polymeric chains resulting in slower viscous relaxation processes. Another finding from these tests is that the relaxation times do not significantly depend on the prescribed strains tested.

3.3. Dynamic mechanical analysis (DMA) under uniaxial compression loading and magnetic fields

Dynamic mechanical analysis is performed to investigate the viscoelastic behaviour of the MREs under uniaxial compression loading and different external magnetic fields. This analysis provides, for the different manufacturing and magnetic conditions tested, the evolution of the storage (E'), loss (E'') and complex (E^*) moduli with the excitation frequency. Another interesting parameter is $\tan\delta = \frac{E'}{E''}$ (loss factor), which is a measure of the ratio between the stored and dissipated energies. Frequency sweeps have been conducted from 0.01 Hz to 16 Hz for different magnetic particles' volume fractions $\phi = \{0, 0.1, 0.2, 0.3\}$ and for axial magnetic flux densities of $B = \{0, 200, 500, 1000\}$ mT. An amplitude of 25 μm (i.e., 2.5% strain) was used. These results are shown in Fig. 4, where the storage modulus, loss modulus and loss factor are depicted for the applied magnetic fields of $B = \{0, 500\}$ mT (see Fig. A.1 in the Appendix for tests at $B = \{200, 1000\}$ mT).

Several findings can be highlighted from these DMA tests. For every B-field (magnetic flux density field) value and for every magnetic particles' concentration, both storage and loss moduli monotonously increase with frequency due to the viscous nature of the MRE samples (i.e., strain rate dependency). The wavy behaviour of the factor suggests that different relaxation mechanisms become excited at different frequencies. The presence of the magnetic particles hinders the mobility of polymeric chains, hence the macroscopic stiffness results to be from two to three times larger than its counterpart without magnetic particles (see further analysis in Table 1). When an external magnetic field is applied (Figs. 4B and A.1), a remarkable stiffening of the MRE samples takes place. This stiffening can be quantified by the magneto-rheological effect defined as $MR_{Effect} = \frac{E'_{B=i}}{E'_{B=0}}$. Thus, the MR_{Effect} ranges from 7.4 to 235.9 for 200 mT and 1000 mT, respectively (see further details in Table 1). In fact, by applying a 1000 mT magnetic field (Fig. A.1), the complex modulus experiences a relevant increase from the order of a few kPa to MPa. Moreover, under magnetic field conditions, $tan\,\delta$ values show an abrupt decrease, indicating that the mechanical behaviour approaches to that of an ideal elastic solid.

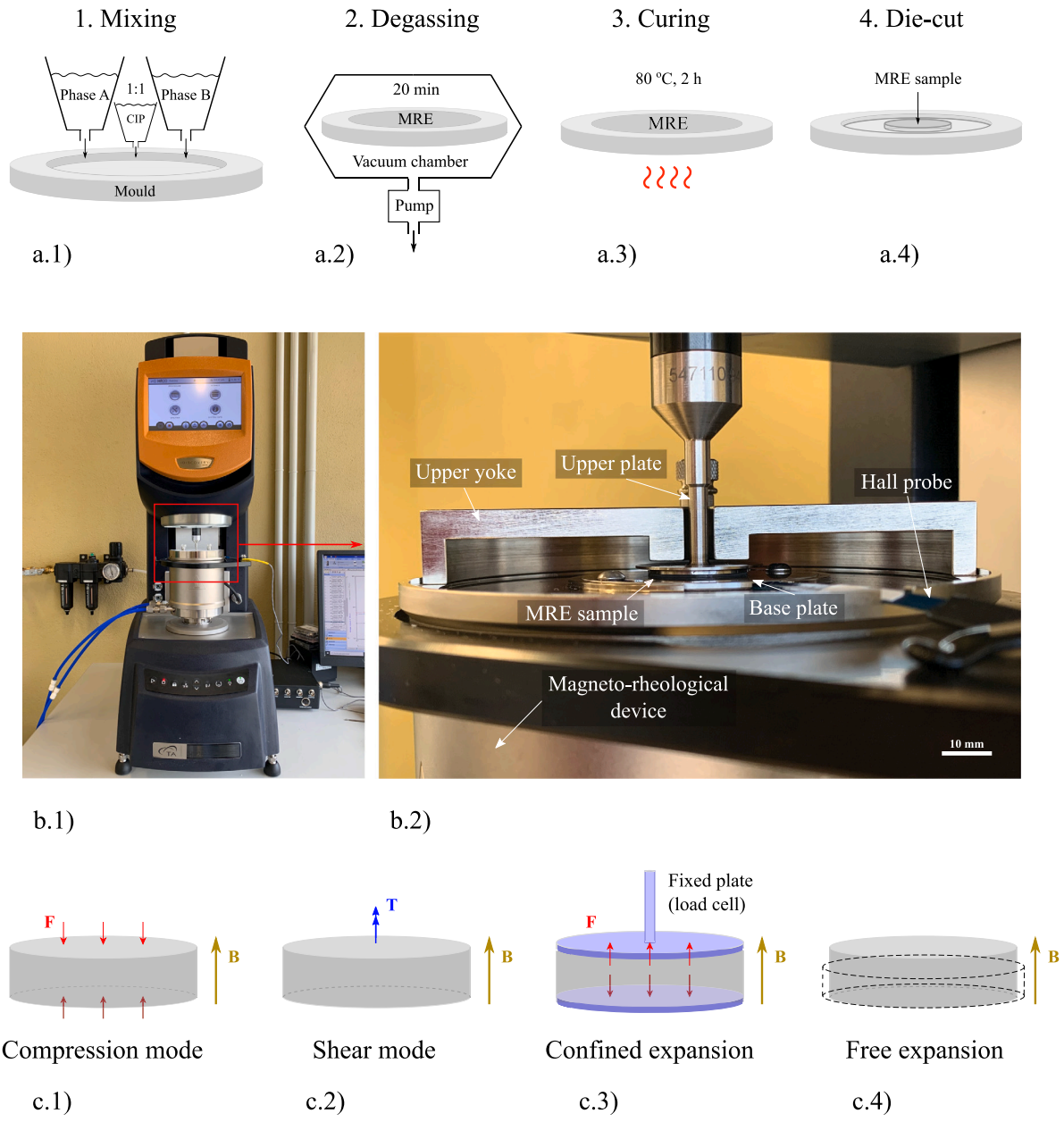

Fig. 1. (a) Scheme of the experimental manufacturing methodology using a mould made of polytetrafluoroethylene (PTFE). Note that ice is used to prevent the chemical reaction during the first synthesis stages. (b) Experimental setup: (b.1) HR-20 rheometre equipped with the magneto-rheological device; (b.2) a detail of the sample placed between the upper plate (geometry) and the lower plate of the magneto-rheological peltier. One half of the upper yoke is removed for better visualisation of the sample region. (c) Scheme of the magneto-mechanical tests performed in this work.

3.4. Novel mechanically confined tests under different magnetic field rates

We have designed experiments where the MRE sample is mechanically confined in the axial direction. While keeping such a mechanical boundary condition, a magnetic field is applied in the axial direction at a given rate. Once a specific targeted magnetic field is reached, this magnetic field is kept constant during certain time (to reach steady state). Note that these experiments have a motivation similar to relaxations tests (here the magnetic field acts as strain). Therefore, the main input in the experiment is the evolution of the magnetic flux density field along time and a mechanical boundary condition equivalent to a permanent unit axial stretch. Then, the upper plate of the rheometre, equipped with an axial load cell, provides the evolution of the axial force (suitably expressed in engineering stress terms) as output. These tests are conducted for four different magnetic rates that are applied until reaching a magnetic field of 1000 mT, which is then kept constant, and for different MREs with magnetic particle's volume fractions of $\phi = \{0.1, 0.2, 0.3\}$. These results are shown in Fig. 5 by means of engineering stress versus time showing average curves and experimental dispersion from a number of six tests per condition.

Each sub-figure in Fig. 5 corresponds to a magnetic field application rate $\dot{B} = \{2, 20, 200, 1000\}$ mT/s and compares the response of different particles' volume fractions. A deep analysis of these results provides several interesting and unexplored observations:

- The increase in engineering stress (and then in axial force) when applying the magnetic field suggests that the MREs tend to expand when subjected to axial magnetic fields (see Section 5 for more details).
- As the magnetic field ramp begins, the axial force evolves in an initially parabolic fashion. However, this tendency is lost in favour of a sigmoidal fashion when larger values of the magnetic field are reached. These tendencies are related to an internal magnetic stress which depends on the magnetic field by a second order function (see

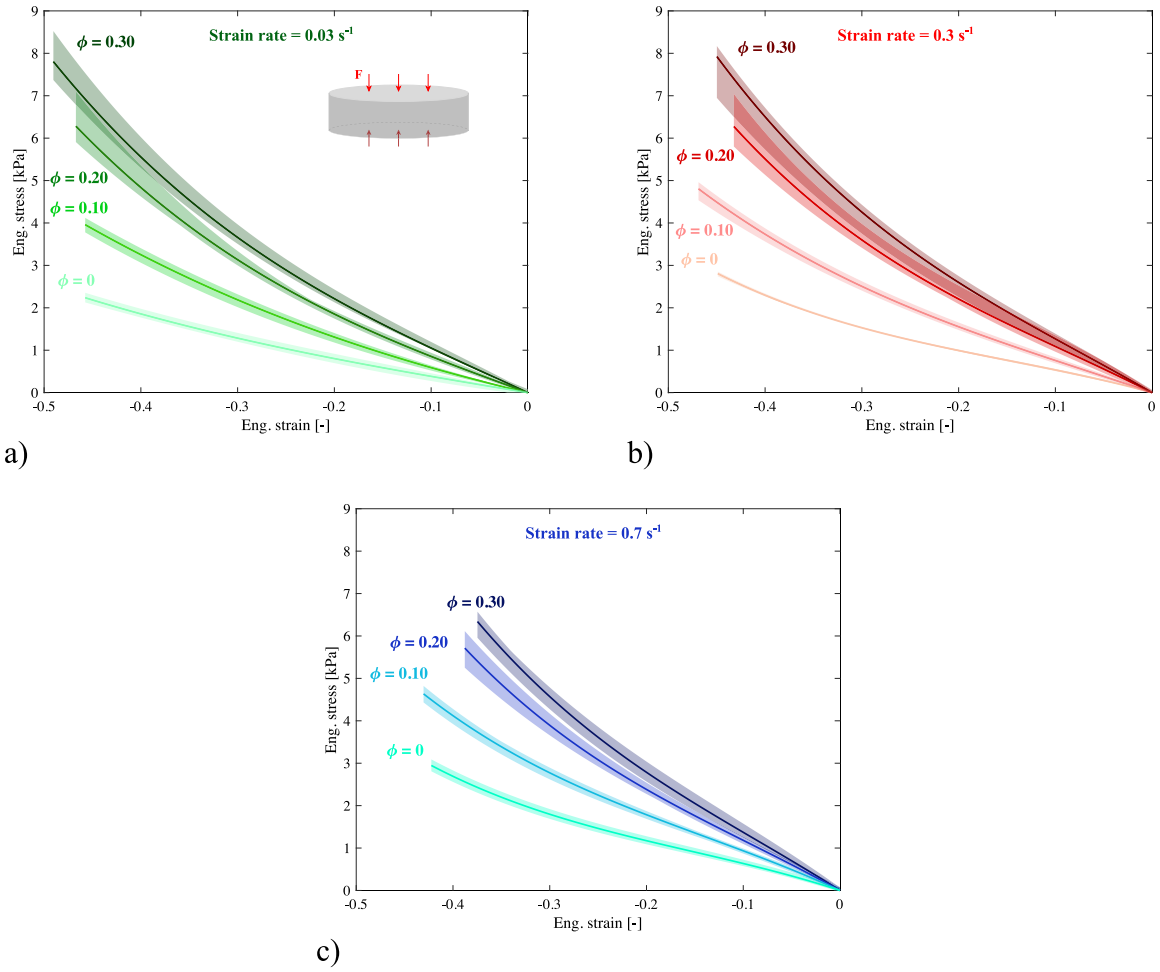

Fig. 2. Experimental results for the uniaxial compression tests upon 1 mm height cylindrical specimens and 20 mm diameter. Engineering stress is plotted against engineering strain for three different strain rates: (a) 0.03, (b) 0.3 and (c) 0.7 s^{-1}, and for magnetic particles' volume fractions of $\phi = \{0, 0.1, 0.2, 0.3\}$. A scatter area around each mean curve is depicted to illustrate the variability of experimental data sets.

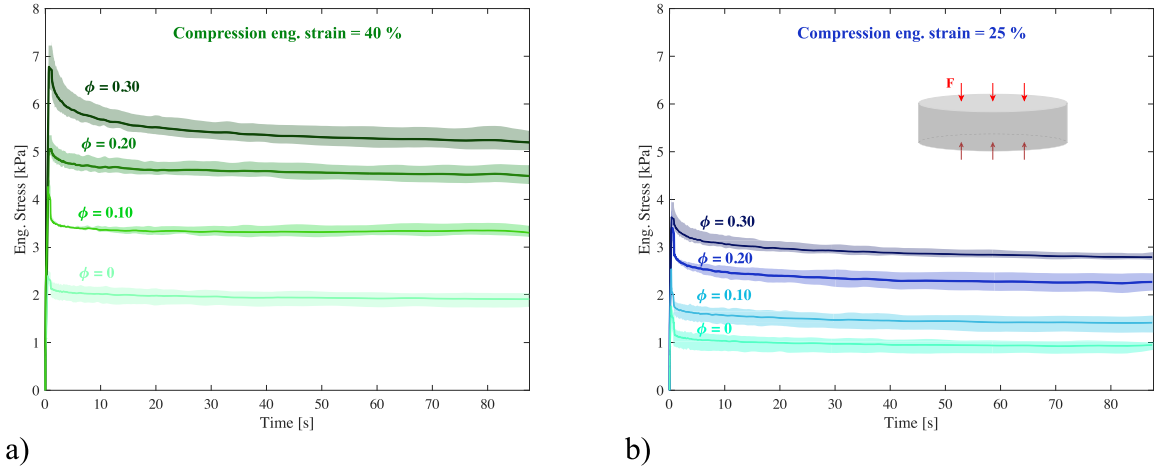

Fig. 3. Experimental results for the relaxation tests upon 1 mm height and 20 mm diameter cylindrical specimens. Engineering stress is plotted against time for (a) 40% and (b) 25% applied strains and magnetic particles' volume fractions of $\phi = \{0, 0.1, 0.2, 0.3\}$. A scatter area around each mean curve is depicted to illustrate the limits of experimental data sets.

modelling approaches in the literature [28,66–69]). This relationship changes at higher magnetic fields due to a nonlinear relationship between particles' magnetisation and magnetic field when approaching to magnetic saturation (see modelling approaches in the literature [70, 71]). Note that although the linear relationship between particles' magnetisation and external magnetic field is lost, the particles do not saturate completely [26].

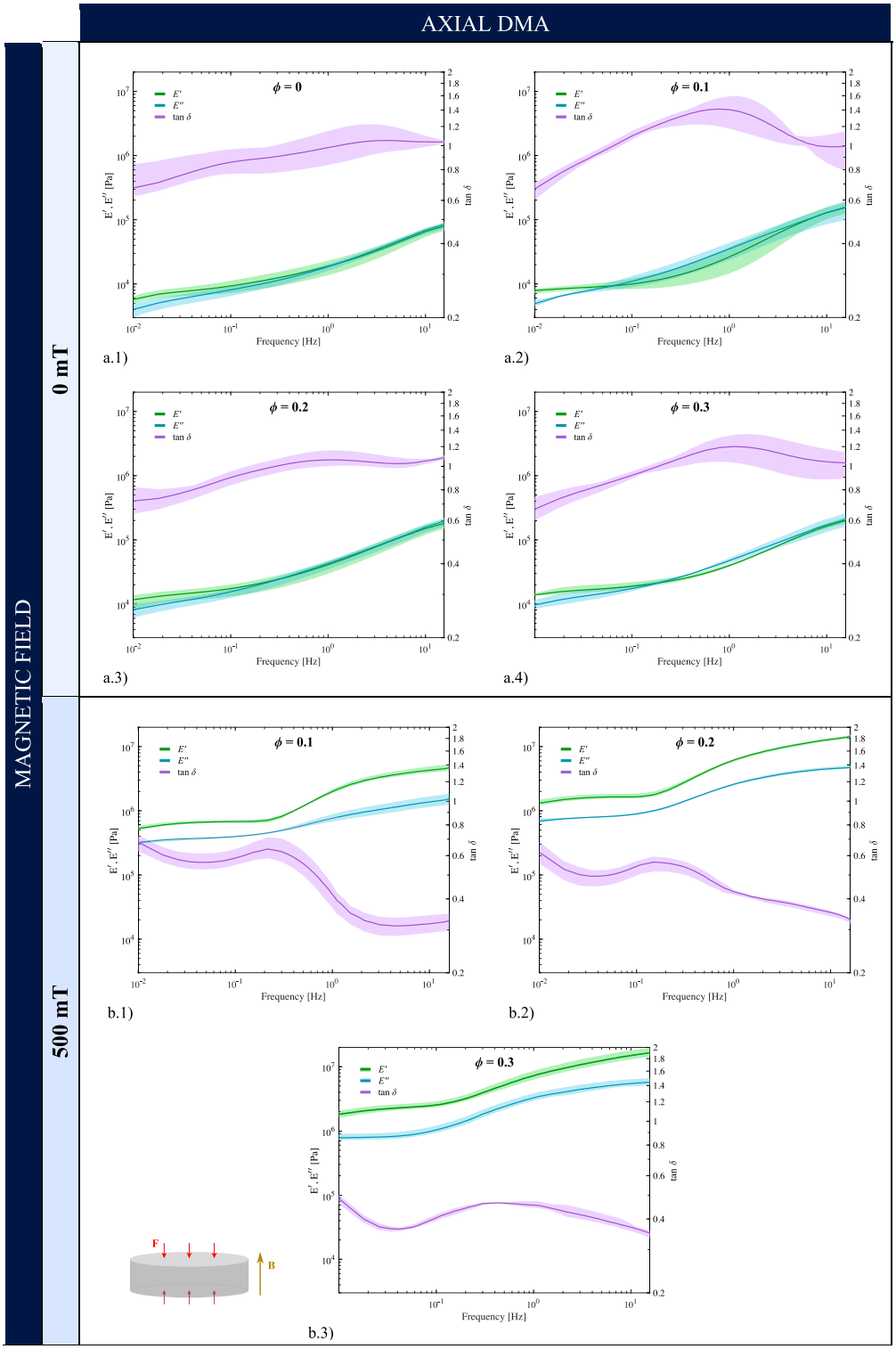

Fig. 4. Experimental results for frequency sweeps from 0.01 to 16 Hz under uniaxial compressive DMA, 1 mm height and 20 mm diameter cylindrical specimens and with magnetic particles' volume fractions of 0, 0.1, 0.2 and 0.3. Storage modulus, loss modulus and loss factor are plotted against frequency. Magnetic fields of (a) 0 mT and (b) 500 mT are externally applied on the samples. Scatter areas around each mean curve are depicted to illustrate the variability of experimental data sets.

• There is a proportional relationship between the maximum stress reached and the magnetic particles' content. This is explained by the higher macroscopic magnetisation of the MRE and the increment of internal dipole–dipole interactions between particles pushing the elastomeric matrix to deform [28,72].

• The maximum stress is reached exactly at the time point when the applied magnetic field reaches its maximum value at low magnetic rates. However, there is a delay in this peak when the magnetic rate is higher. Such a delay is related to a rate dependency on particles' magnetisation, which presents a limit rate to polarise due to magnetic viscosity [73–76]. This phenomenon is governed by the thermal activation of the magnetisation over local energy barriers arising from varied sources, e.g., shape and anisotropy of the particles. The coefficient of

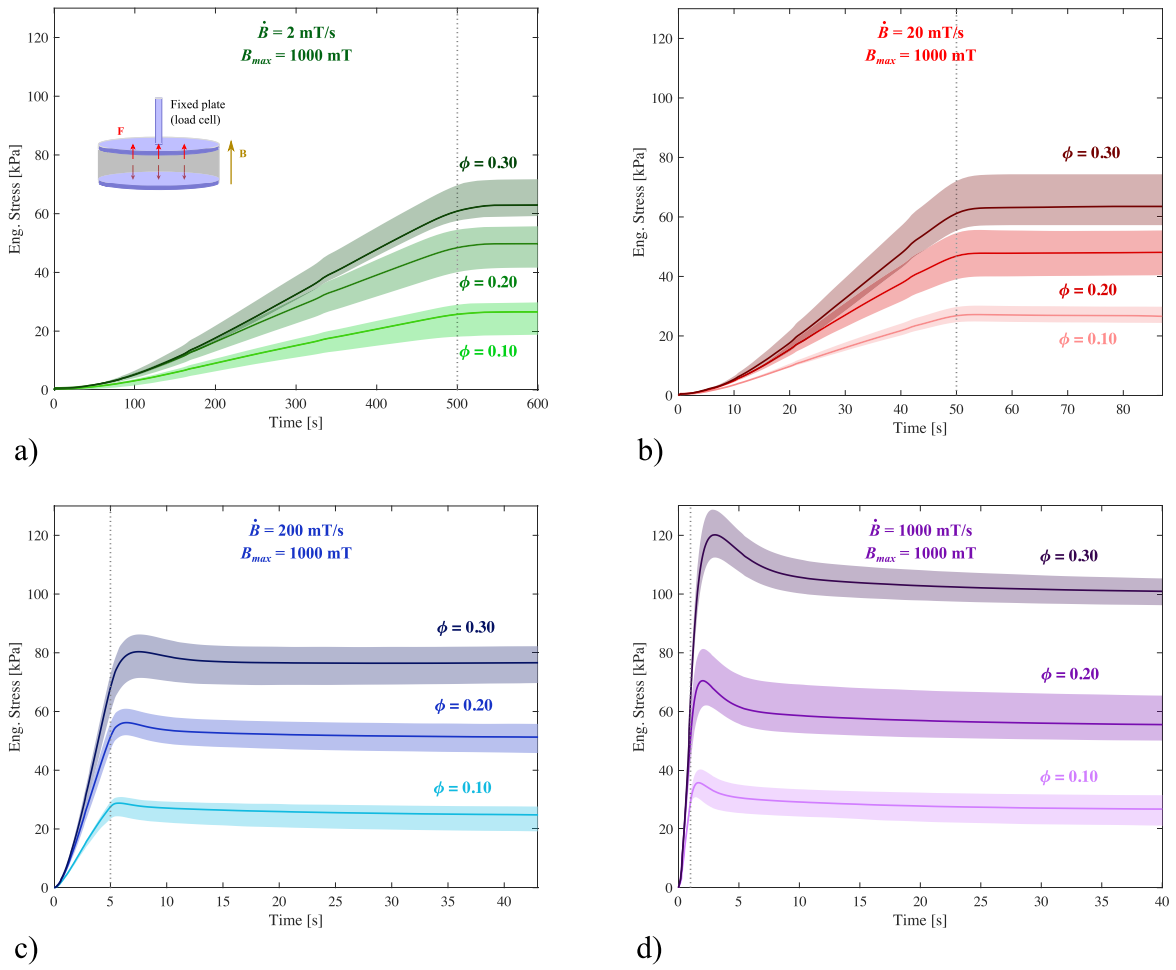

Fig. 5. Experimental results for the application of a 1000 mT magnetic field in the form of temporal ramps with different application rates: (a) 2 mT/s, (b) 20 mT/s, (c) 200 mT/s and (d) 1000 mT/s. After reaching the targeted magnetic field, indicated by a dotted vertical line, the magnetic field is kept constant for a given time. Confined axial deformation is imposed during the whole experiment as mechanical boundary condition. The samples used are cylindrical MREs with height 1 mm and diameter 20 mm, which are manufactured with different magnetic particles' volume fractions of $\phi = \{0.1, 0.2, 0.3\}$. Engineering stress is plotted against time covering the temporal application of the ramp plus an additional period where the field is held constant at 1000 mT. Scatter areas around each mean curve are depicted to illustrate the variability of experimental data sets.

magnetic viscosity has been widely used to take into account these mechanisms, being the temperature a major factor [77].

• At the lower magnetic rates, although mechanical strain rate effects were expected at these time scales, the maximum stress reached is the same. These tendencies can be explained by making use of a recently developed microstructural-based model for soft magneto-active polymers [28]. In this regard, the macroscopic stress is understood as the contribution of a magnetic stress due to dipole–dipole interactions between particles and the external magnetic field, and the contribution of a mechanical stress due to deformation of the polymeric matrix. Thus, when fixing the axial stretch and applying the external magnetic field, the particles magnetise leading to interaction forces and reaching an equilibrium state. In such a scenario, the device is measuring the transmitted magnetic forces within the MRE and the viscoelastic response is balanced without relevant implications. However, at higher magnetic rates (200 and 1000 mT/s), there is a remarkable effect in the macroscopic response of the structure leading to higher maximum stresses when increasing the magnetic rate. This response may be explained by the microstructural stiffening of the polymeric matrix resulting in a sudden collapse of magnetic particles, which are prevented from a proper arrangement and leads to a microstructural blockage. This phenomenon will need further investigation by more advanced microstructural based models.

• After reaching the maximum stress value, while such stress is kept constant for tests at low magnetic rates, the MREs experience a relaxation response at higher magnetic rates. In other words, at slow enough magnetic rates the particles are able to reach the final equilibrium state (i.e., magnetic particles' distribution under the applied field). Therefore, the purely elastic and viscous contributions of the elastomeric matrix stress balance each other until full microstructural relaxation. Moreover, at higher magnetic rates, the previously mentioned microstructural blockage is followed by a mechanical relaxation of the elastomeric matrix relaxing such a state. Note that this statement is supported by the relaxation time scales observed in these experiments, which are in the same order than the characteristic times identified from the relaxation tests (Fig. 3).

• The final observation relates to the long term stresses reached after complete relaxation (steady state). These values are notably larger at higher magnetic rates, suggesting that the MRE encounters alternative equilibrium states (i.e., magnetic particles' distributions) depending on the historical evolution of the microstructural deformation. From a mechanical perspective, this effect can be understood as a yielding-like process where the particles and the matrix get blocked under the applied magnetic field.

4. Magneto-mechanical characterisation under shear loading

This section addresses the experimental results related to the magneto-mechanical behaviour of the MREs tested under different torsional shear loading conditions. Contrary to the compression tests,

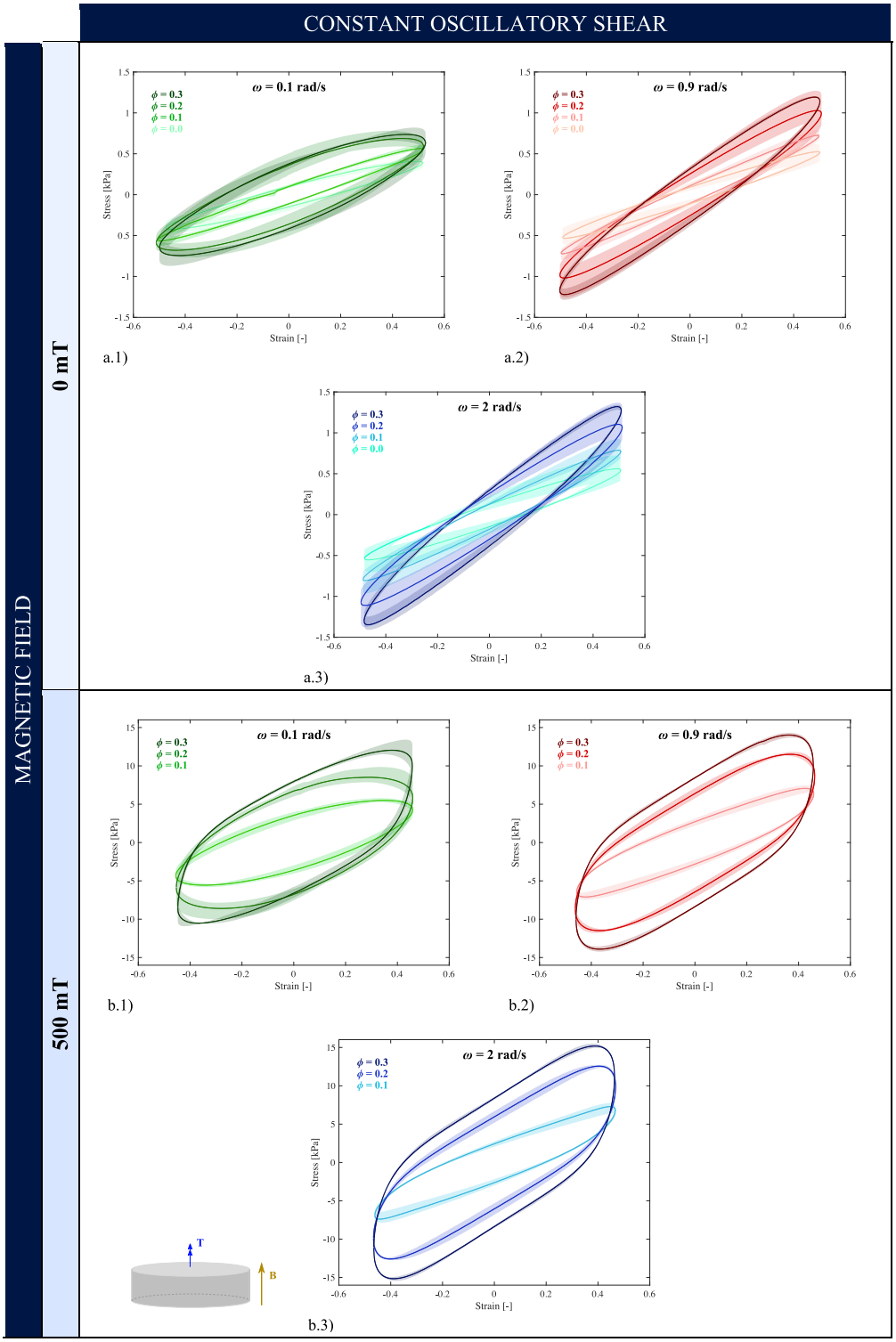

Fig. 6. Experimental results for oscillatory shear rheology on 1 mm height and 20 mm diameter cylindrical specimens with magnetic particles' volume fractions of $\phi = 0, 0.1, 0.2, 0.3$ and angular velocities of: (a) 0.1 rad/s, (b) 0.9 rad/s, and (c) 2 rad/s. Azimuthal shear stress τ is plotted against shear strain $\gamma = r\frac{\alpha}{H}$, with radial coordinate $r = \frac{2}{3}r_{max}$. Magnetic fields of (a) 0 mT and (b) 500 mT are externally applied on the samples. Scatter areas around each mean curve are depicted to illustrate the variability of experimental data sets.

no lubricant is used as no slip between the sample and the upper and bottom plates is desired. In this regard, Walter et al. [78,79] have thoroughly examined the boundary conditions in experimental magneto-mechanical rheology, highlighting their importance and providing guidance to achieve slip-free interfaces between the plates and the sample when working in shear mode. The sticky nature of the elastomeric matrix ensures the contact at the interfaces preventing from wall slippage. Such a contact is characterised by the azimuthal shear stress (τ) on the contact interfaces, which varies with radial coordinate r (i.e., zero at $r = 0$ and maximum at $r_{max} = 10$ mm). In this work, we refer the stress and strain values to a radial coordinate of $r = \frac{2}{3}r_{max}$ (DIN 53018). From the torsion angle (α) and torque (M) on the rheometer

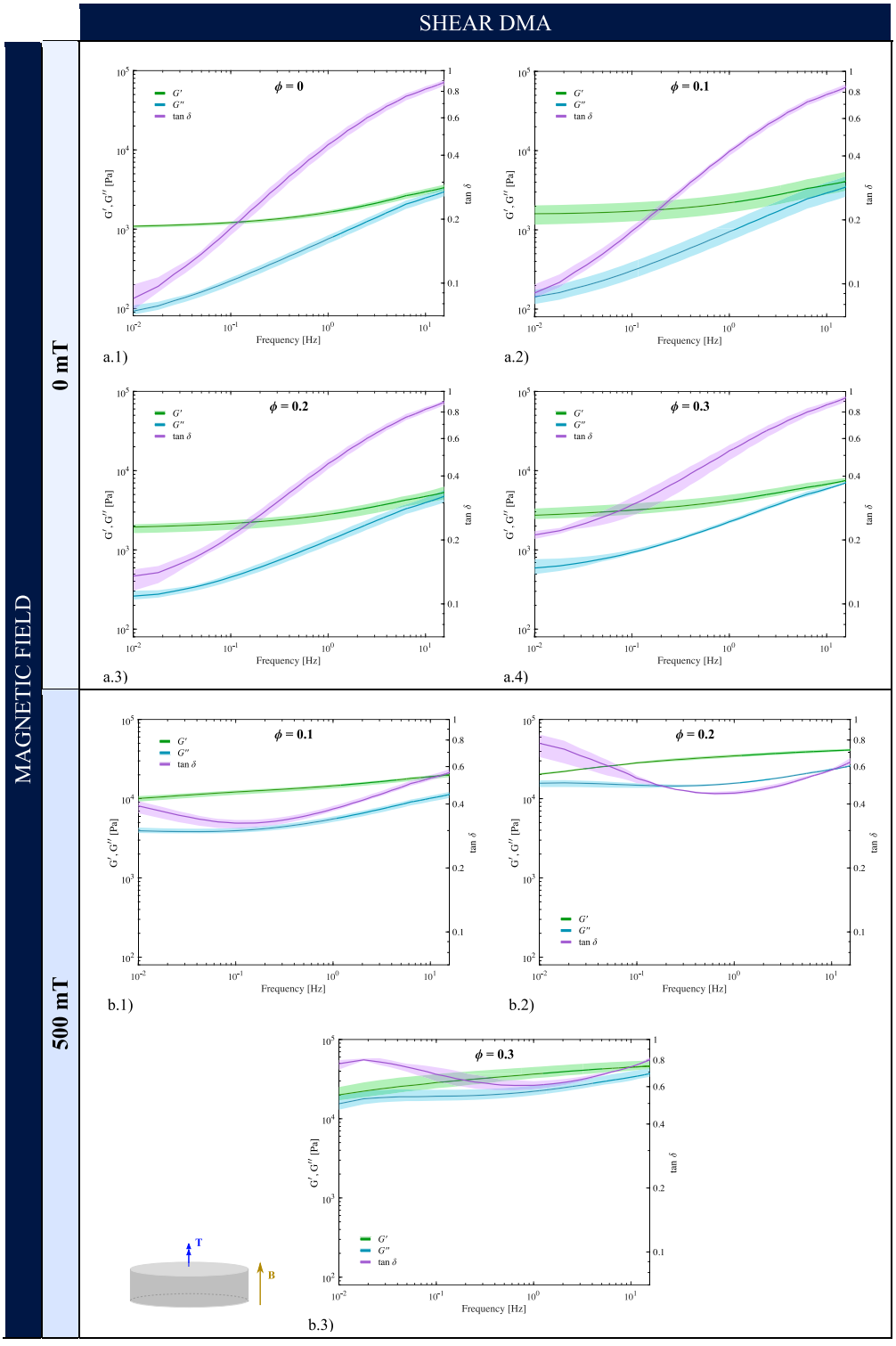

Fig. 7. Experimental results for frequency sweeps from 0.01 to 16 Hz under shear mode on 1 mm height and 20 mm diameter cylindrical specimens and with magnetic particles' volume fractions of: 0, 0.1, 0.2 and 0.3. Storage modulus, loss modulus and loss factor are plotted against frequency. Magnetic fields of (a) 0 mT and (b) 500 mT are externally applied on the samples. Scatter areas around each mean curve are depicted to illustrate the variability of experimental data sets.

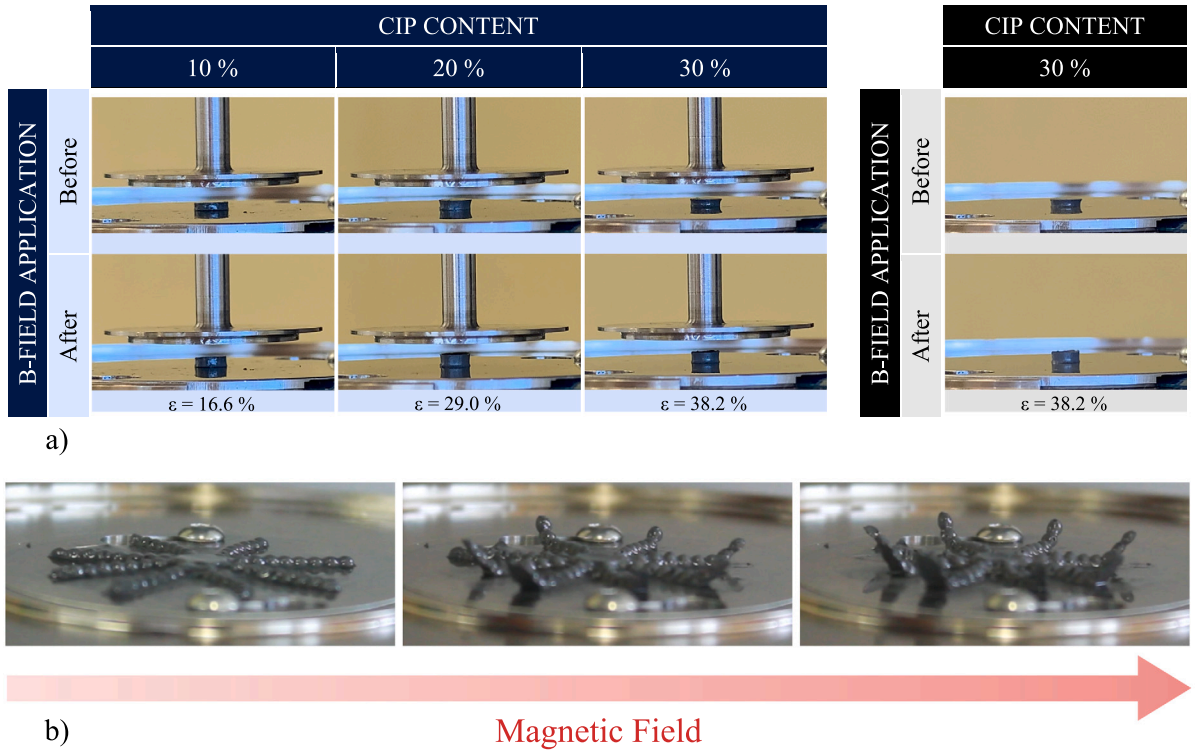

Fig. 8. (a) Mechanical response of MREs under the application of an external magnetic field with free boundary conditions and for different particles' volume fractions $\phi = \{0.1, 0.2, 0.3\}$. The MRE samples have diameter 4 mm and height 1 mm. The table on the right hand side shows the exact same test for $\phi = 0.3$ without the presence of the upper plate. The magnetic field was imposed as a temporal ramp to a maximum value of 250 mT. (b) Mechanical response of a star-shape MRE with $\phi = 0.3$ under the application of an external magnetic field with free boundary conditions. The sample was manufactured following the same moulding procedure shown in Fig. 1a.

axis, and assuming that the torsion angle is linearly distributed along the axial coordinate of the sample, we compute the stress and strain for the representative points as:

$$\tau(M) = \frac{4M}{3\pi r_{max}^3}, \qquad \gamma(\alpha) = \frac{2}{3}\frac{\alpha r_{max}}{H}, \tag{1}$$

with H being the initial height of the sample.

4.1. Constant oscillatory shear

To start with, constant amplitude and frequency oscillatory finite shear tests are conducted on cylindrical MRE samples. In these experiments, the upper plate applies a torque on the cylindrical sample to perform a sine-shaped angular displacement. This deformation profile is defined for a 48% strain and fixed angular velocities of $\omega = \{0.1, 0.9, 2\}$ rad/s. The strain amplitude has been chosen so as the sample deforms beyond the infinitesimal strain regime. The axial position of the upper plate is initially established to ensure sample-plate contact with negligible compressive axial stress. Moreover, these tests are carried out under different magnetic flux densities of $B = \{0, 200, 500, 1000\}$ mT. An intriguing point is that, when applying the external magnetic fields, the samples tend to expand leading to an effective pre-compression state in the axial direction. One may argue that such an effect could influence the magnetorheological effect analysed in this section. This effect is deeply analysed in Section 5 and proved to be negligible. Finally, as for compression tests, we have performed six repetitions for each test condition to ensure repeatability.

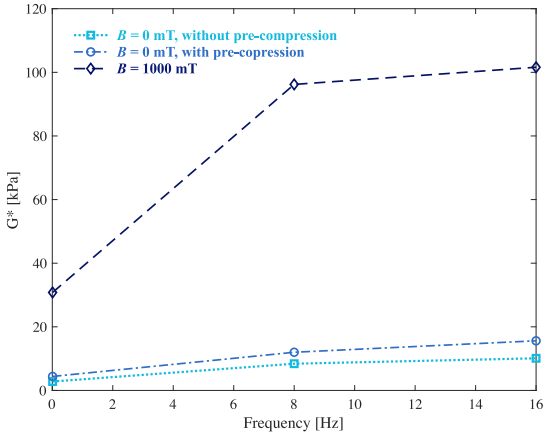

Fig. 9. Experimental results comparing the effects of three different conditions on frequency sweeps tests with frequencies of $f = \{0.01, 8, 16\}$ Hz: experiment with high magnetic field (1000 mT), experiment without magnetic field but with a pre-strain producing the same axial force as with magnetic field, and experiment without magnetic field and without pre-compression.

Fig. 6 (and Fig. A.3 in the Appendix) show, for the different magnetic field conditions, the results in the form of shear stress versus shear strain for the chosen angular velocities (each sub-figure) and

Table 1
Quantitative summary and comparison of the trends revealed by mechanical and magneto-mechanical uniaxial compression tests on MRE samples with magnetic particles' volume fractions of $\phi = \{0, 0.1, 0.2, 0.3\}$ and magnetic fields of $B = \{0, 200, 500, 1000\}$ mT. Characteristic relaxation time is defined as the time that it takes to accomplish a 63.21% of the total stress relaxation. All the results provided correspond to the mean values over the six experimental repetitions.

Case study		CIPs amount (ϕ)			
Parameter	Test conditions	**0**	**0.1**	**0.2**	**0.3**
MECHANICAL TESTS - COMPRESSION					
Characteristic relaxation time [s]	Mean value	1.0	1.1	4.7	6.5
Tangent modulus at 10% strain, E [kPa]	0.03 s^{-1}	4.0	6.5	9.0	10.8
	0.3 s^{-1}	4.7	7.6	10.6	12.6
	0.7 s^{-1}	5.6	8.5	11.4	13.4
Tangent modulus at 30% strain, E [kPa]	0.03 s^{-1}	5.2	9.6	14.7	16.4
	0.3 s^{-1}	6.3	10.7	16.0	19.2
	0.7 s^{-1}	7.3	11.4	17.7	20.8
CIPs stiffening ratio at 10% strain, $\frac{E_{\phi=i}}{E_{\phi=0}}$ [–]	0.03 s^{-1}	–	1.6	2.3	2.7
	0.3 s^{-1}	–	1.6	2.3	2.7
	0.7 s^{-1}	–	1.5	2.0	2.4
CIPs stiffening ratio at 30% strain, $\frac{E_{\phi=i}}{E_{\phi=0}}$ [–]	0.03 s^{-1}	–	1.8	2.8	3.1
	0.3 s^{-1}	–	1.7	2.6	3.1
	0.7 s^{-1}	–	1.6	2.4	2.8
MAGNETO-MECHANICAL TESTS - COMPRESSION					
Complex modulus E^* [kPa] for 0 mT	0.01 Hz	7	9	14	17
	8 Hz	83	162	195	213
	16 Hz	116	221	265	291
Complex modulus E^* [kPa] for 200 mT	0.01 Hz	–	195	308	432
	8 Hz	–	1102	2380	4147
	16 Hz	–	1265	2740	4767
Complex modulus E^* [kPa] for 500 mT	0.01 Hz	–	618	1490	1973
	8 Hz	–	4133	13160	15169
	16 Hz	–	4800	14840	17222
Complex modulus E^* [kPa] for 1000 mT	0.01 Hz	–	697	2188	3421
	8 Hz	–	4873	14862	18613
	16 Hz	–	5369	15963	19890
MR Effect, $\frac{E'_{B=200\text{mT}}}{E'_{B=0\text{mT}}}$ [–]	0.01 Hz	–	20.6	21.9	25.7
	8 Hz	–	9.0	16.4	26.1
	16 Hz	–	7.4	13.7	21.4
MR Effect, $\frac{E'_{B=500\text{mT}}}{E'_{B=0\text{mT}}}$ [–]	0.01 Hz	–	67.0	112.7	130.4
	8 Hz	–	36.3	92.8	97.1
	16 Hz	–	29.0	76.5	79.3
MR Effect, $\frac{E'_{B=1000\text{mT}}}{E'_{B=0\text{mT}}}$ [–]	0.01 Hz	–	79.7	181.1	235.9
	8 Hz	–	41.2	105.0	118.9
	16 Hz	–	32.5	79.1	86.7

for magnetic particle's volume fractions of $\phi = \{0, 0.1, 0.2, 0.3\}$. This representation is often known as the Lissajous figure, which conveys interesting information, e.g., about the energy lost by viscous dissipation mechanisms, in a visual way.

Clear trends can be found form these constant oscillatory shear tests. For all the experimental conditions, larger maximum stresses are reached for higher amounts of magnetic particles. This is due to the same stiffening effect of magnetic particles formerly described in compression tests, where magnetic fillers hinder the displacement of polymeric chains leading to increased macroscopic stiffness. Moreover, when external magnetic field is applied, the MRE sample undergoes additional stiffness as a result of internal magnetic interaction forces, with values of the MR_{Effect} up to 12.3 (see Table 2 for further detail). As the magnetic field increases, it can also be concluded that the Lissajous loops progressively lose their quasi-ellipsoidal shape, in agreement with a previous work by Dargahi et al. [52]. This latter point is associated to a pronounced nonlinear response of the composite when increasing the presence of stiffer particles, as observed in compression (Fig. 2) and tensile tests [23]. Other major factors influencing the mechanical response of the sample are viscous mechanisms. In this regard, maximum stresses appear with the highest deformation rate showing a clear strain rate dependency, similarly as observed in compression tests.

4.2. Dynamic mechanical analysis (DMA) under shear loading and magnetic fields

These experiments can be understood as an extension of constant oscillatory shear ones, where different angular velocities are consecutively applied. For this analysis, as similarly done for compression, we analyse the evolution of the storage (G'), loss (G'') and complex (G^*)

Table 2
Quantitative summary and comparison of the trends revealed by mechanical and magneto-mechanical shear tests on MRE samples with magnetic particles' volume fractions of $\phi = \{0, 0.1, 0.2, 0.3\}$ and magnetic fields of $B = \{0, 200, 500, 1000\}$ mT. All the results provided correspond to the mean values over the six experimental repetitions.

Case study		CIPs amount (ϕ)			
Parameter	Test conditions	**0**	**0.1**	**0.2**	**0.3**
MAGNETO-MECHANICAL TESTS - SHEAR					
Complex modulus G^* [kPa] for 0 mT	0.01 Hz	1.1	1.6	2.0	2.8
	8 Hz	3.6	4.4	5.7	8.4
	16 Hz	4.4	5.3	7.0	10.1
Complex modulus G^* [kPa] for 200 mT	0.01 Hz	–	3.7	8.1	8.3
	8 Hz	–	8.1	16.8	18.8
	16 Hz	–	9.3	19.3	21.6
Complex modulus G^* [kPa] for 500 mT	0.01 Hz	–	10.8	24.2	25.3
	8 Hz	–	20.8	45.5	54.3
	16 Hz	–	22.8	48.4	59.1
Complex modulus G^* [kPa] for 1000 mT	0.01 Hz	–	12.7	25.4	30.8
	8 Hz	–	27.2	69.8	96.2
	16 Hz	–	30.1	73.9	101.6
CIPs stiffening ratio, $\frac{G^*_{\phi=i}}{G^*_{\phi=0}}$ [–], $B = 0$ mT	0.01 Hz	–	1.5	1.8	2.5
	8 Hz	–	1.2	1.6	2.3
	16 Hz	–	1.2	1.6	2.3
MR Effect, $\frac{G'_{B=200\text{mT}}}{G'_{B=0\text{mT}}}$ [–]	0.01 Hz	–	2.2	3.8	2.7
	8 Hz	–	1.9	3.0	2.2
	16 Hz	–	1.8	2.8	2.1
MR Effect, $\frac{G'_{B=500\text{mT}}}{G'_{B=0\text{mT}}}$ [–]	0.01 Hz	–	6.3	10.5	7.3
	8 Hz	–	5.3	8.9	6.8
	16 Hz	–	4.8	7.5	6.1
MR Effect, $\frac{G'_{B=1000\text{mT}}}{G'_{B=0\text{mT}}}$ [–]	0.01 Hz	–	6.9	7.4	5.5
	8 Hz	–	7.0	14.4	13.1
	16 Hz	–	6.4	12.4	11.5

shear moduli with the excitation frequency. The loss factor in shear mode reads as $\tan\delta = \frac{G''}{G'}$.

Frequency sweeps have been conducted from 0.01 Hz to 16 Hz for different magnetic particles' volume fractions $\phi = \{0, 0.1, 0.2, 0.3\}$ and for axial magnetic inductions of $B = \{0, 200, 500, 1000\}$ mT. Note that the used elastomeric matrix presents no significant hardening/softening with strain amplitude (see Fig. A.5a in Appendix). However, in accordance with other works in the literature [52], there is a strong effect of the strain amplitude when testing under external magnetic fields, due to changes in the relative positions of the magnetised particles that modulate dipole–dipole interactions (see Fig. A.5b in Appendix). Therefore, the amplitude of the harmonic oscillations is defined as 0.05 rad (~30% strain) to limit this effect (stronger at lower strain amplitudes). The results of these experiments are shown in Fig. 7, where the storage modulus, loss modulus and loss factor are plotted versus frequency for 0 mT and 500 mT magnetic fields (see additional tests in Fig. A.2 in the Appendix for 200 mT and 1000 mT magnetic fields).

Diverse findings can be stated from these frequency sweeps. For all the test conditions, the complex modulus increases with angular velocity, showing the strain rate dependency of the MREs under shear loading. The maximum stiffness increase of the material due to this effect is observed for MRE samples with $\phi = 0.3$ and a magnetic field of $B = 1000$ mT, presenting a value of $\Delta G^* = 71$ kPa with respect to the smallest oscillation frequency at these conditions. In addition, the loss factor provides relevant information about the viscoelastic behaviour of the material. As for the compression mode tests, $tan\,\delta$ decreases with larger B-field inductions, denoting that material stiffening due to magneto-rheological effect brings it closer to a purely elastic and non-viscous behaviour (see a quantitative comparison in Table 2). Another remark for high magnetic field (1000 mT) is related to the storage and loss moduli at low frequencies, where both present an abrupt decrease, see Fig. A.2b. This tendency is more notable for the higher magnetic particles' volume fractions.

5. Discussion

This section addresses a comprehensive discussion focused on the interplays between rate and magnetic dependences. First, two tables gathering major quantitative tendencies from all the original experiments performed are presented as a comparative framework (e.g., complex elastic moduli, tangent moduli at different strain values, magneto-rheological effect, loss factor and dimensionless ratios). Such tables give raise to a set of discussions with special focus on the underlying multifunctional phenomena. Then, complementary magneto-mechanical tests are introduced to clarify the MREs response under free mechanical boundary conditions and external magnetic fields. Moreover, and in order to confirm that the influence of the induced axial stress on shear DMA tests under magnetic fields is negligible, we have performed additional experiments with $B = 0$ mT with the same pre-compression as for the analogous magneto-mechanical experiment. Finally, we have performed additional mechanically confined tests with a maximum external magnetic field of 200 mT to further analyse magnetic and deformation rate couplings.

Table 1 synthesises major tendencies from axial compression tests. First, characteristic stress relaxation time is found to be significantly influenced by the amount of magnetic particles, with times from around 1 s for smaller amounts up to 6.5 s for the highest concentrations. In this regard, the polymeric network can be understood as a mix of a cross-linked network and free elastomeric chains. When the MRE is quickly deformed, the cross-linked network pushes the remaining elastomeric chains resulting in a higher instantaneous stiffness. These free chains tend to slip within the polymeric network relaxing the stiffness along time. However, the presence of the stiff magnetic particles hinders such a relaxation leading to higher characteristic times. Although this effect is quite limited at low particles' content (i.e., $\phi = 0.1$), it is very significant at higher ones. Moreover, relaxation times are found to not significantly change with the imposed strain, i.e., the tendencies found on relaxation tests for 25% and 40% strain present no significant changes. This indicates that alternative compression states do not lead to different viscous relaxation mechanisms, thus presenting similar relaxation processes. Still associated with viscous effects, all the MREs tested show a direct relationship between apparent stiffness and strain rate. Furthermore, when externally applying a magnetic field, the magneto-mechanical coupling plays a major role determining the response of the material. To frame this coupling in a quantitative fashion, representative mechanical parameters are shown at low, medium and high excitation frequencies in DMA $f = \{0.01, 8, 16\}$ Hz. Furthermore, the relative influence of the magnetic field on the mechanical properties of the composite is defined by means of the so-called magneto-rheological effect ratio (MR_{Effect}). For large amount of magnetic fillers, the MRE becomes up to 235.9 times stiffer. Also, note that the MR effect is around twice larger for smaller excitation frequencies. All in all, such a broad set of quantitative results extracted from the charts from previous sections allows for easy comparison of the behaviour of the MRE in compression mode. Note that the amount of magnetic fillers encounters certain limitations when large amounts are added to the composite. For this reason, MRE samples with very high content of particles are mechanically less efficient than their counterparts with fewer fillers. Kallio et al. [45] reported that BASF

SQ CIP has a critical particle volume concentration (CPVC) of 29.1%, defined from the apparent and bulk densities of CIPs for the particles to be in contact. Thus, the MR effect shows a maximum at the CPVC value. Our results, for both axial compression and shear modes (see Table 2), fulfil this tendency, i.e., the increase in the MR effect from magnetic particle's volume fraction $\phi = 0.1$ to $\phi = 0.2$ is bigger than that from $\phi = 0.2$ to $\phi = 0.3$. For compression, the averaged MR effect increase (ΔMR_{Effect}), for the three excitation frequencies shown, from $\phi = 0.1$ to $\phi = 0.2$ and for 1000 mT is of $\Delta MR_{Effect} = 70.6$, whereas it is only an increase of $\Delta MR_{Effect} = 25.4$ from $\phi = 0.2$ to $\phi = 0.3$. In shear mode, changes of $\Delta MR_{Effect} = 4.6$ and $\Delta MR_{Effect} = -1.4$, respectively, take place. These analysed ΔMR_{Effect} suggest that the CPVC is close to $\phi = 0.3$, hence the magneto-rheological stiffening is less efficient for larger amounts of magnetic fillers.

Table 2 gathers the results from the magneto-mechanical shear tests in an analogous way. A first look into these quantitative results suggests that the MR effect strongly depends on the deformation mode. The DMA frequency sweeps under the same magnetic fields shows a magneto-rheological stiffening substantially smaller in shear mode than in axial compression mode. In this regard, in shear mode the stiffness of the MRE is improved within one order of magnitude, whereas in axial compression it increased up to two orders of magnitude. These observations must be carefully discussed as they are the result of different effects. On the one hand, it must be noted that the external magnetic field is axially applied (i.e., in compression direction) during both types of tests. This axial magnetic field promotes a strong interaction of the magnetic particles in axial direction which, apart from dipole–dipole interaction forces, results into particles alignment into chain-like microstructures (note that the extremely soft nature of the elastomer used allows this). Therefore, it seems reasonable that external magnetic fields result in a higher resistance to deformation in axial mode than in shear. On the other hand, the application of the axial magnetic field while confining the axial deformation of the sample leads to a pre-compression state. Thus, when analysing the MREs under axial loading, a relevant increase in stiffness is observed due to not only magnetic interactive forces but also to such a pre-compression state. We have, however, focused on a detailed study of the effect of this axially induced stress state (see following discussion and complementary experiments).

In the literature, it has been reported that, under the application of external magnetic fields, MREs can either compress or expand. On the one hand, some early works state that MREs contract along the field direction as the particles feel attracted between each other [10,80,81]. On the other hand, expansion is reported to happen under certain conditions, e.g., when particles are isotropically distributed [82]. This point of discussion is directly related to the pre-compression states arising from the applied magnetic field, that can be easily intuited by the experiments conducted in Fig. 8. In this work, by means of the mechanically confined tests under magnetic fields from Section 3.4 monitoring compressive axial forces, it is clear that the MRE samples tend to expand. To clarify this question, we have performed additional tests under free mechanical boundary conditions (i.e., no mechanical confinement in the axial direction and lubrication on the sample-machine interface on its lower face) to investigate the free deformation of samples of 4 mm diameter and 1 mm height. We have chosen these smaller-diameter specimens to ensure that the magnetic field remains homogeneous through the composite despite not using the upper yoke (neglecting magnetic fringing effects). In Fig. 8a, pictures of the specimens before and after the application of a 250 mT field are shown for magnetic particle's volume fractions of $\phi = \{0.1, 0.2, 0.3\}$. An additional experiment for $\phi = 0.3$ with the upper plate shifted upwards is presented just to show that it does not affect the magneto-mechanical deformation mechanism due to upper plate magnetisation. From these results, it is found that the MRE sample macroscopically expands up to strains of 38.2% for $\phi = 0.3$. Moreover, note that this macroscopic response is the result of microscopic interactions competing with structural responses. To clearly show such effects, we have included a free expansion test on a star-like sample made of $\phi = 0.3$ MRE (see Fig. 8b). Under the application of an external magnetic field, a structural response is observed where the particles try to form chains along the magnetic field (i.e., paramagnetic torque [83] governs over dipole–dipole interactions).

This magnetically induced axial deformation may also question the interpretation of the results obtained for the shear study. From a microscopic magneto-mechanical approach, Danas et al. [72] studied the influence of positive and negative pre-strain (i.e., elongation and compression) of the sample, observing from experiments overall elongations for compressive pre-stresses, and contractions for tensile ones. Vatandoost et al. [84] reported how pre-strain affects stiffening, dampening and MR effect of MREs samples in axial compression. In our frequency sweep tests for shear deformation mode (see Section 4.2), and despite initially setting the position of the upper plate to impose no pre-strain, significant compressive axial forces arise when applying the magnetic field. To clarify how this interplays with shear stiffness of the sample (complex shear modulus), we have performed three additional tests which are collected in Fig. 9. In this figure, we compare the shear complex modulus obtained from a shear frequency sweep for three different frequencies and three representative conditions: (i) MRE under null magnetic field and subjected to negligible axial force (i.e., pre-compression); (ii) MRE under an externally applied magnetic field; (iii) MRE under null magnetic field and subjected to an axial force equivalent to the one observed during the magneto-mechanical test performed in condition (ii) (i.e., equivalent pre-compression state due to the applied magnetic field). These results show small change in stiffness due to the pre-compression arising from magnetic interactions, whereas a significant increase in stiffness due to the application of the external magnetic field is found. In this regard, there is a maximum discrepancy of 5 kPa for 16 Hz between the shear complex modulus for the test without magnetic field and with the pre-compression. Nevertheless, the increase in the modulus is much bigger when comparing these with the one obtained under an external magnetic field, $\Delta G^* = 90$ kPa.

Another question from the analysis of the magneto-mechanical experiments is related to the results presented in Section 3.4 for mechanically confined tests under different magnetic field rates. Special attention has been conferred to the macroscopic effect found for the fastest field rates (200 and 1000 mT/s), where a kind of magneto-mechanical relaxation process is observed. Provided that the magnetic particles require a certain amount of magnetic energy and time to reorganise from their initial positions to a new spatial arrangement, we believe that, for sufficiently high field rates, a microstructural blockage occurs. Since magnetic interactions between the magnetic particles are transmitted in the form of mechanical forces to the carrier matrix, this microstructural collapse is macroscopically detected by a larger axial force on the specimen. Furthermore, as the amount of magnetic particles increases, this effect becomes more significant, hence larger axial forces are measured. However, there is still an open question: what is the influence of the magnitude of the magnetic field induction in this phenomenon? To shed light on this matter, we have conducted complementary mechanically confined tests to a smaller maximum magnetic field of 200 mT, for slow and fast field rates of 5 mT/s and 200 mT/s, respectively. The results, depicted in Fig. A.6 for

the $\phi = 0.3$ MRE samples, confirm the relaxation-like mechanisms identified, as well, for smaller magnetic fields. In what concerns the time delay between the end of the magnetic field ramp and the peak in the stress response, it does change for this smaller magnetic field: now the delay is of 0.3 s, whereas it was of 2.5 s for the $B_{max} = 1000$ mT counterpart. The relaxation characteristic time after the peak is similar for the tests up to 1000 mT, which strongly suggests a governing role of mechanical relaxation of the carrier matrix during this process. Overall, mechanically confined tests under certain magnetic field rates give rise to remarkable prospects within further computational research. This problem could be suitably studied in the close future by full-field modelling approaches accounting for viscous, mechanical and magnetics interactions. In addition, these experiments highlight the importance of accounting for such rate-dependent mechanisms when designing specific applications. These mechanisms, as shown, can be explored by determining the transient and steady states in the magneto-mechanical responses.

Mechanically confined tests under different magnetic field rates have been presented as novel experiments. For the sake of better conceptualisation of these tests, applying a magnetic field with axially confined samples is equivalent to a relaxation test but, instead of imposing uniaxial compression by external mechanical boundary conditions, the mechanical forces are imposed by internal interaction forces arising from the application of an external magnetic field. Liao et al. [85] worked on a similar idea by establishing relationships between the magnetic field induction and the pre-strain of MRE samples. We believe that our experiments enable for in detail studying the magneto-mechanical principles that originate at the micro-scale level and determine the macroscopic response. Thus, despite constraining the macroscopic axial deformation, microstructural phenomena drive particles to new states of equilibrium while interacting with the viscoelastic matrix. In addition, under specific conditions (e.g., high particle concentrations, strong magnetic fields), these fillers can collide. All in all, these magneto-mechanical interplays are difficult to detail and need to be addressed from macroscopic measurements.

6. Conclusions

The multifunctional nature of magnetorheological elastomers (MREs) has revolutionised the fields of soft robotics and bioengineering, providing smart structures whose mechanical properties and deformation can be controlled remotely by making use of external magnetic fields. To date, there were unresolved questions preventing the full understanding of the underlying mechanisms of MREs, especially on the importance of magneto-mechanical rate dependences and their interplays. To answer these questions, in this work, we provide an unprecedented experimental characterisation of a soft MRE considering more than 100 experimental conditions combining different mechanical deformation modes and magnetic loading. The experimental campaign includes monotonous uniaxial compression at different deformation rates and magnetic conditions, magneto-mechanical DMA tests, relaxation tests, oscillatory shear tests at different deformation rates and magnetic conditions, magneto-mechanical shear frequency sweep tests, and novel magneto-mechanical experiments. These results are first presented by a full characterisation framework for an extremely soft MRE composed of a PDMS elastomeric matrix and soft magnetic iron particles. Then, we provide a quantitative discussion on the magneto-mechanical coupling and complete the characterisation with complementary experiments to support the findings and help explain the multifunctional mechanisms behind the behaviour of the MREs tested.

The mechanical and magnetic rate-dependent mechanisms have been proved to be quite significant in the structural response of MREs. Both macroscopic stiffness and mechanical viscous relaxation mechanisms can be tuned by adjusting the amount of magnetic particles and the applied magnetic field. Magnetic viscosity, however, depends on the nature of the magnetic particles to overcome thermodynamic barriers. These mechanisms lead to a history-dependent behaviour of the MRE. Vibration absorbers made of MREs [33,35,36] and biocompatible substrates for cell culture stimulation [50,86] are applications that can benefit from tuning these material characteristics. Overall, the experiments provided in this work show a wider tuning span when designing applications for MREs working in axial compression than in shear mode. Starting from 1–4 kPa, the mechanical properties of the material can be tuned within a wide range. This adaptability makes it ideal to be used as biological substrate for cell migration research. For instance, its fast viscous relaxation acts in favour of filopodia-mediated cell migration, as stated by Adebowale et al. [86].

Although a comprehensive experimental characterisation is provided herein, some aspects related to microstructural features during the deformation mechanisms explored needs of further investigation. In this regard, the work presented opens the door for modelling approaches addressing these questions and offers a new starting point for constitutive theories bringing together a wide set of characterisation data.

CRediT authorship contribution statement

M.A. Moreno: Investigation, Experimental methodology, Formal analysis, Writing – original draft, Writing – review & editing. **J. Gonzalez-Rico:** Investigation, Experimental methodology, Writing – review & editing. **M.L. Lopez-Donaire:** Investigation, Experimental methodology, Writing – review & editing. **A. Arias:** Investigation, Formal analysis, Writing – review & editing. **D. Garcia-Gonzalez:** Conceptualisation, Investigation Experimental methodology, Formal analysis, Writing – original draft, Writing – review & editing, Funding acquisition.

Declaration of competing interest

The authors declare that they have no known competing financial interests or personal relationships that could have appeared to influence the work reported in this paper.

Acknowledgements

The authors acknowledge support from the European Research Council (ERC) under the European Union's Horizon 2020 research and innovation programme (grant agreement No. 947723, project: 4D-BIOMAP). MAM acknowledges support from the Ministerio de Ciencia, Innovacion y Universidades, Spain (FPU19/03874) and DGG acknowledges support from the Talent Attraction grant (CM 2018 - 2018-T2/IND-9992) from the Comunidad de Madrid. The authors thank the discussion with Xavier Trepat and Raimon Sunyer on elastomeric materials for their use in cellular applications and material supply. The authors thank great discussions with Sergio Lucarini on magneto-mechanical couplings and microstructural-based explanations.

Appendix. Supplemental results

See Figs. A.1–A.6.

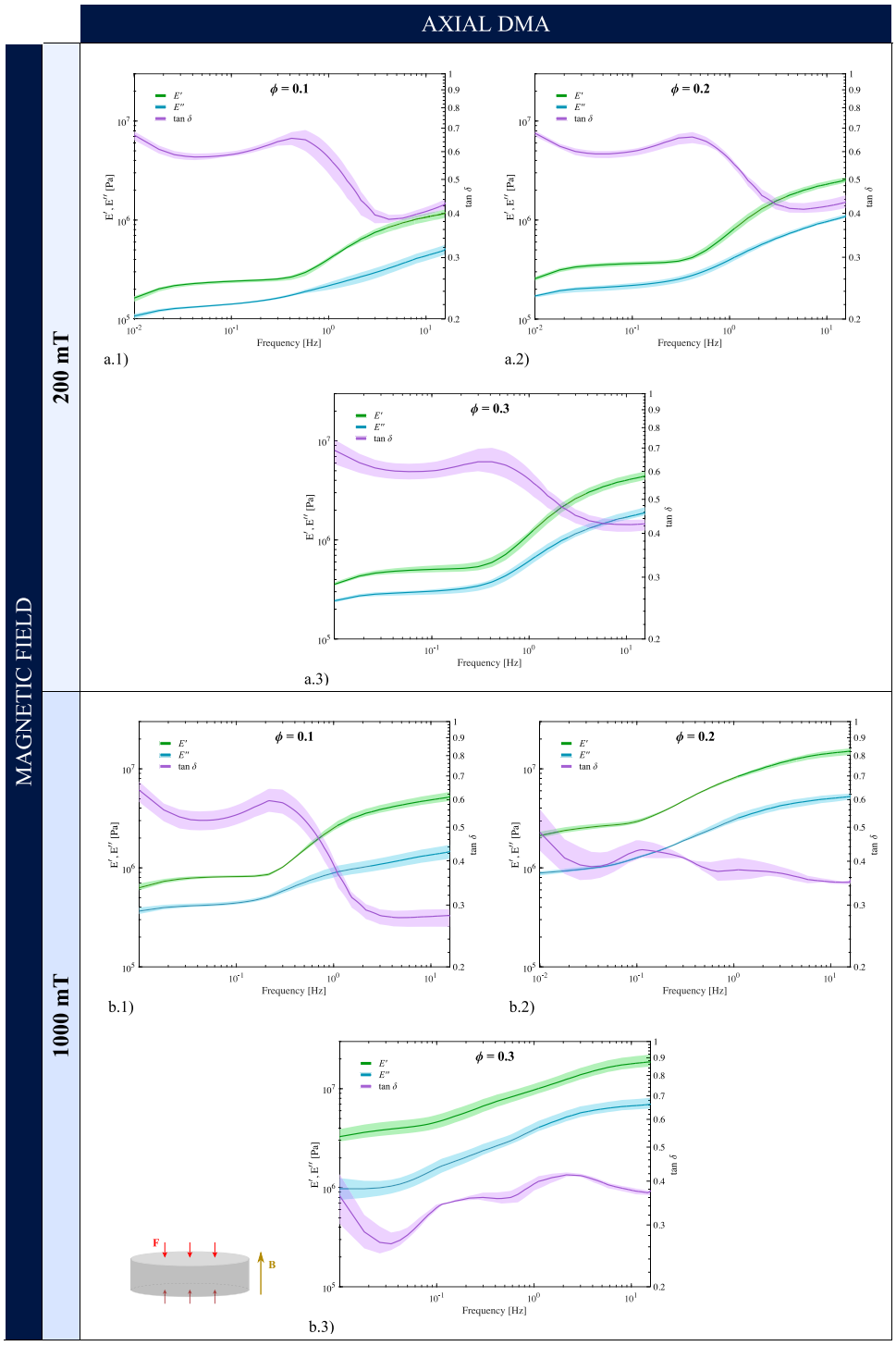

Fig. A.1. Experimental results for frequency sweeps from 0.01 to 16 Hz under uniaxial compressive DMA, 1 mm height and 20 mm diameter cylindrical specimens and with magnetic particles' volume fractions of 0, 0.1, 0.2 and 0.3. Storage modulus, loss modulus and loss factor are plotted against frequency. Magnetic fields of (a) 200 mT and (b) 1000 mT are externally applied on the samples. Scatter areas around each mean curve are depicted to illustrate the variability of experimental data sets.

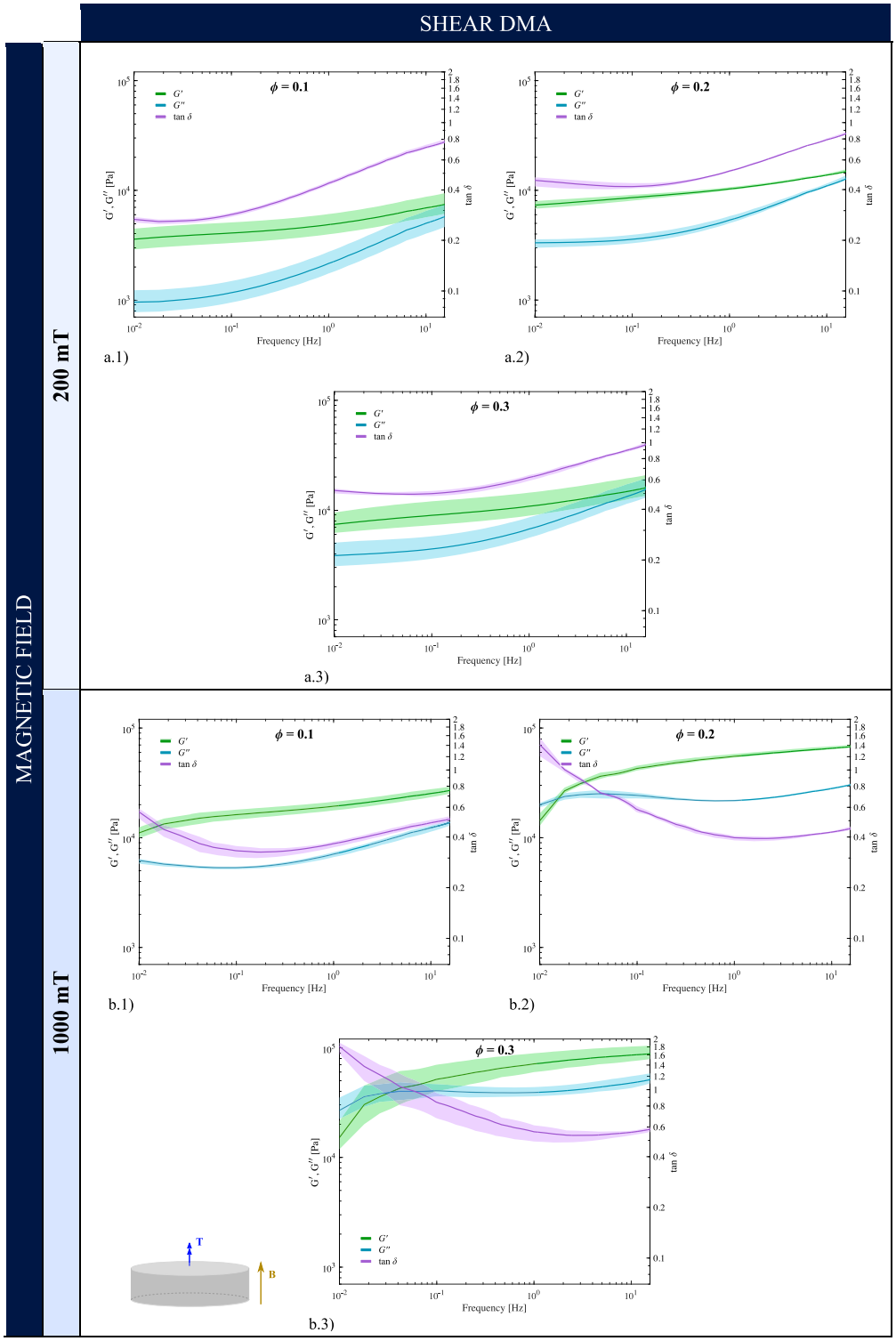

Fig. A.2. Experimental results for frequency sweeps from 0.01 to 16 Hz under shear mode on 1 mm height and 20 mm diameter cylindrical specimens and with magnetic particles' volume fractions of: 0, 0.1, 0.2 and 0.3. Storage modulus, loss modulus and loss factor are plotted against frequency. Magnetic fields of (a) 200 mT and (b) 1000 mT are externally applied on the samples. Scatter areas around each mean curve are depicted to illustrate the variability of experimental data sets.

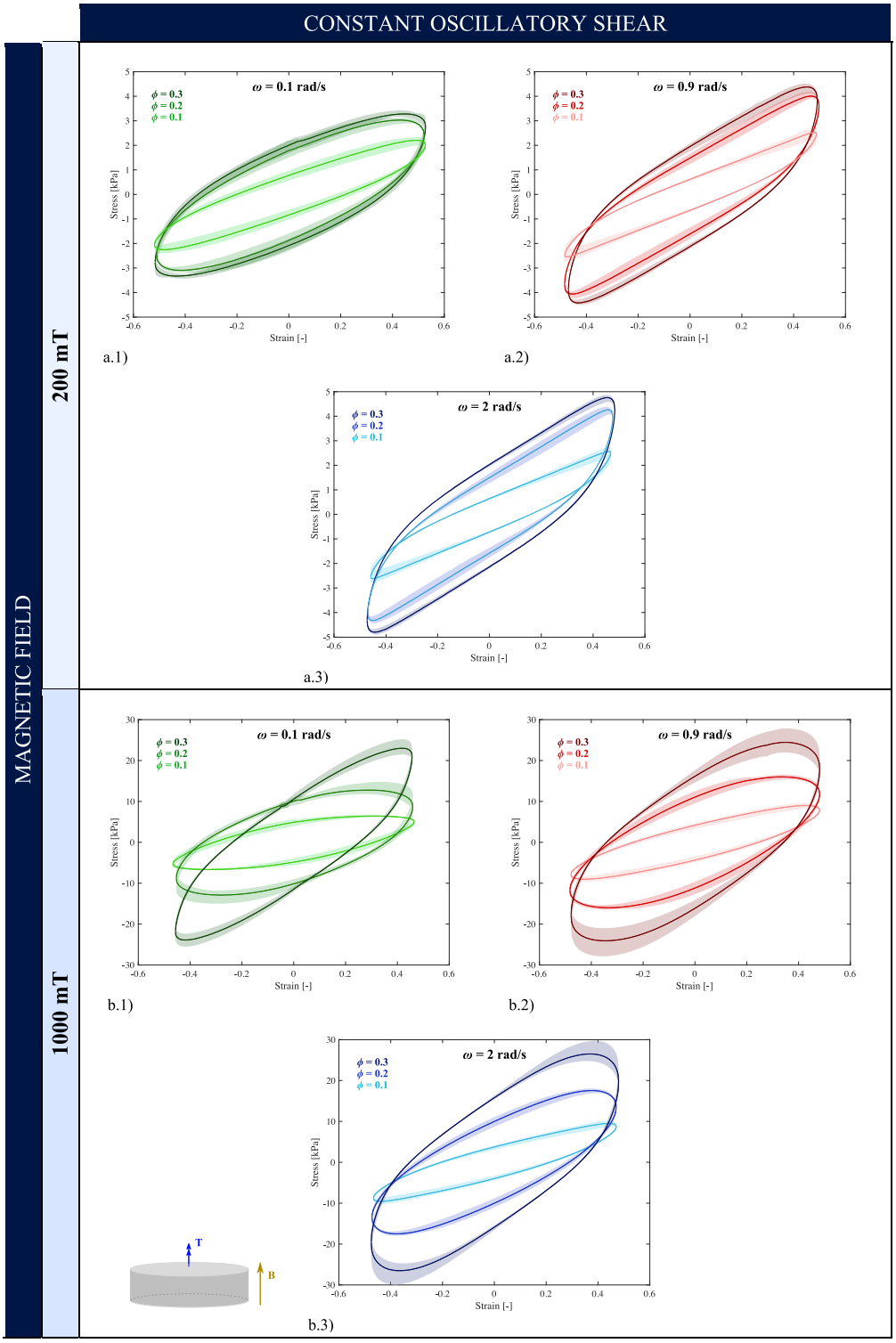

Fig. A.3. Experimental results for oscillatory shear rheology on 1 mm height and 20 mm diameter cylindrical specimens with magnetic particles' volume fractions of $\phi = 0, 0.1, 0.2, 0.3$ and angular velocities of: (a) 0.1 rad/s, (b) 0.9 rad/s, and (c) 2 rad/s. Azimuthal shear stress τ is plotted against shear strain $\gamma = r\frac{\alpha}{H}$, with radial coordinate $r = \frac{2}{3}r_{max}$. Magnetic fields of (a) 200 mT and (b) 1000 mT are externally applied on the samples. Scatter areas around each mean curve are depicted to illustrate the variability of experimental data sets.

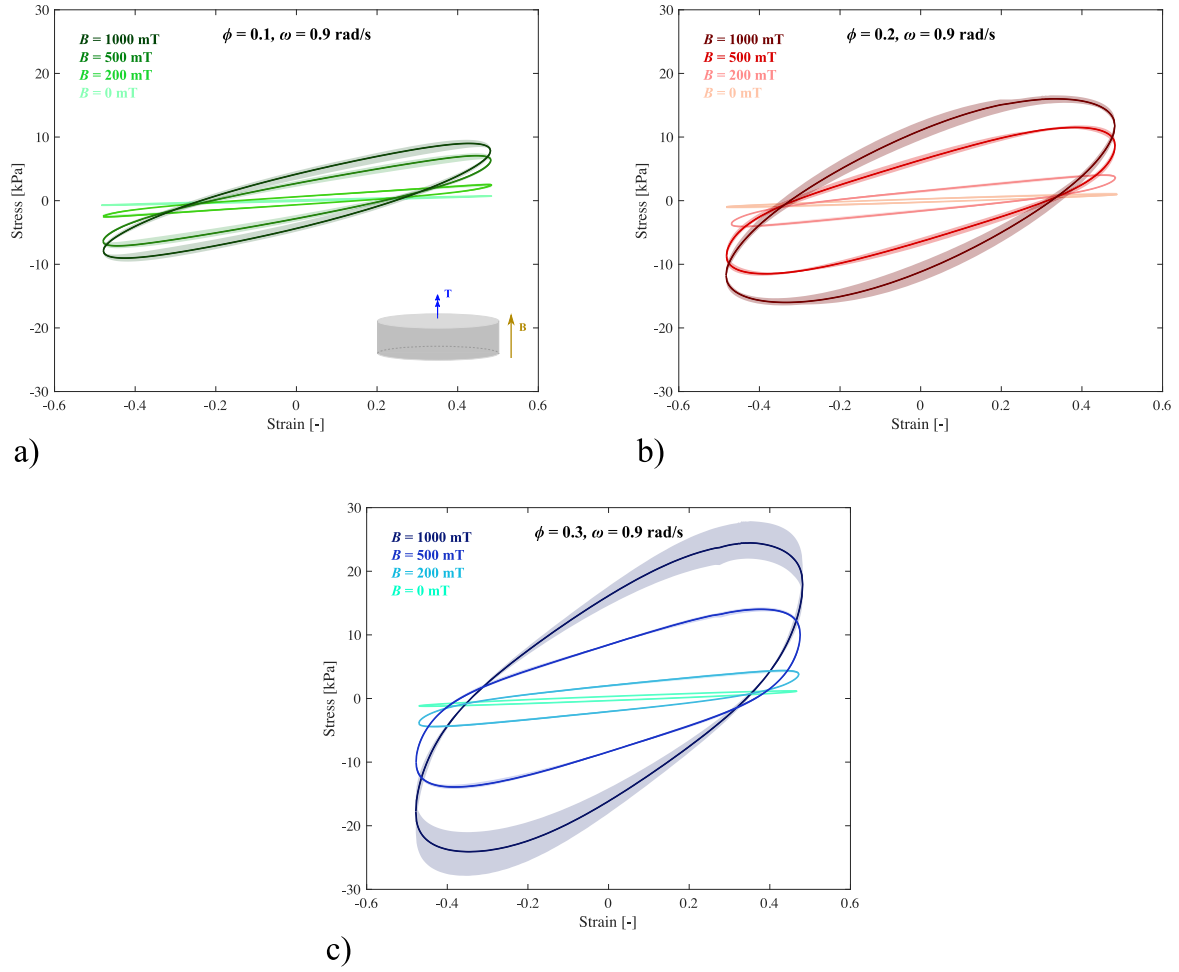

Fig. A.4. Alternative visualisation of the results from the oscillatory shear tests. Curves for magnetic fields $B = \{0, 200, 500, 1000\}$ mT are represented together for fixed magnetic particle's volume fractions of $\phi = \{0.1, 0.2, 0.3\}$ and angular velocity of 0.9 rad/s.

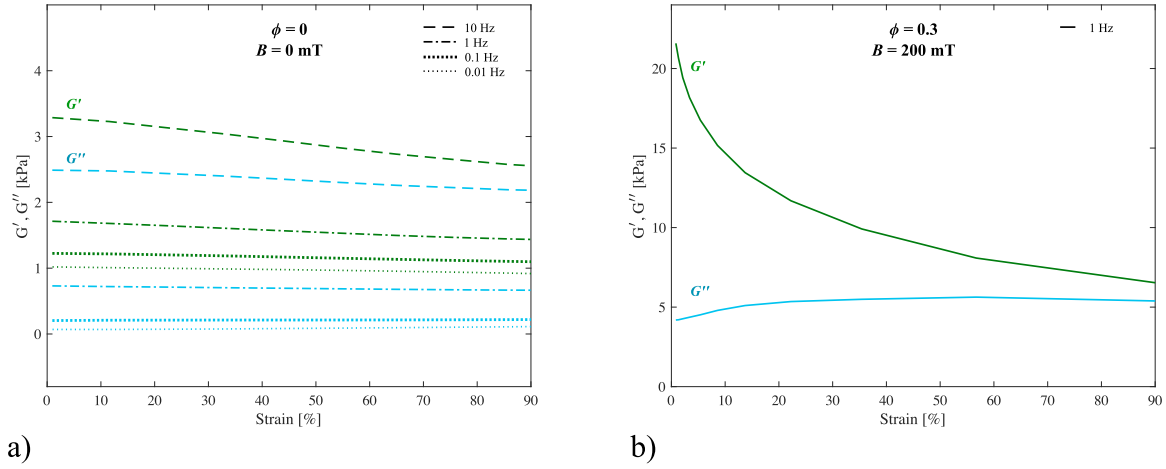

Fig. A.5. Amplitude sweeps to determine the influence of the strain amplitude in shear mode. (a) With null magnetic field and frequencies of $f = \{0.01, 0.1, 1, 10\}$ Hz; (b) with a magnetic field of 200 mT and angular velocity 1 Hz.

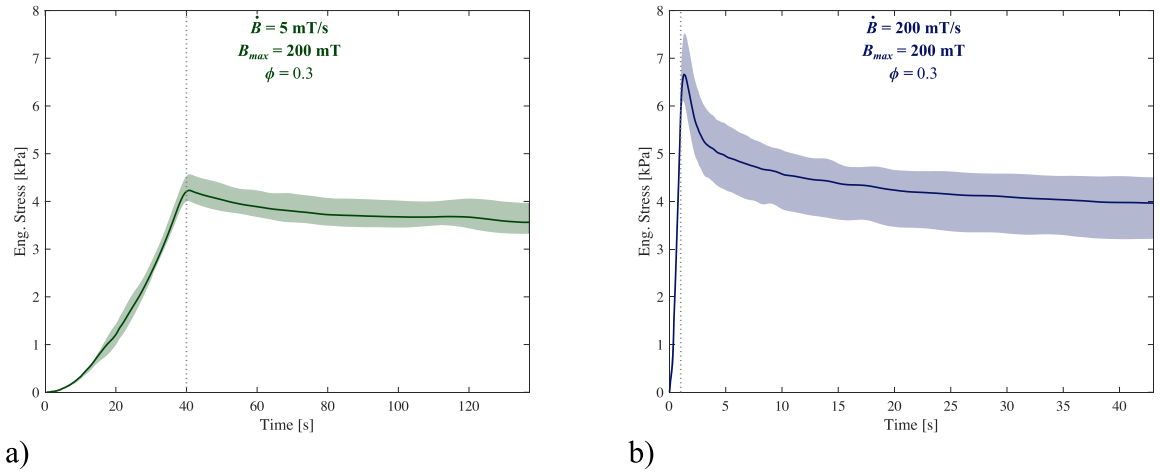

Fig. A.6. Experimental results for the application of a 200 mT magnetic field in the form of temporal ramps with different application rates: (a) 200 mT/s, (b) 5 mT/s. After reaching the targeted magnetic field, indicated by a dotted vertical line, the magnetic field is kept constant for a given time. Confined axial deformation is imposed during the whole experiment as mechanical boundary condition. The samples used are cylindrical MREs with height 1 mm and diameter 20 mm, which are manufactured with a magnetic particles' volume fraction of $\phi = 0.3$. Engineering stress is plotted against time covering the temporal application of the ramp plus an additional period where the field is held constant at 200 mT. Scatter areas around each mean curve are depicted to illustrate the variability of experimental data sets.

References

[1] Bastola AK, Hossain M. Enhanced performance of core-shell hybrid magnetorheological elastomer with nanofillers. Materials Letters 2021;297. http://dx.doi.org/10.1016/j.matlet.2021.129944.

[2] Fischer L, Menzel AM. Magnetostriction in magnetic gels and elastomers as a function of the internal structure and particle distribution. J Chem Phys 2019;151(11):114906. http://dx.doi.org/10.1063/1.5118875.

[3] Han Y, Mohla A, Huang X, Hong W, Faidley LE. Magnetostriction and field stiffening of magneto-active elastomers. Intl J Appl Mech 2015;07(01):1550001. http://dx.doi.org/10.1142/S1758825115400013.

[4] Ubaidillah, Sutrisno J, Purwanto A, Mazlan SA. Recent progress on magnetorheological solids: materials, fabrication, testing, and applications. Advanced Engineering Materials 2014. http://dx.doi.org/10.1002/adem.201400258.

[5] Xu Y, Liao G, Liu T. Magneto-sensitive smart materials and magnetorheological mechanism. 2019, http://dx.doi.org/10.5772/intechopen.84742.

[6] Rabinow J. The magnetic fluid clutch. Trans Amer Inst Electric Eng 1948;67(2):1308–15. http://dx.doi.org/10.1109/T-AIEE.1948.5059821.

[7] Mangal SK, Sharma V. On state rheological characterization of MRF 122EG fluid using various techniques. Mater Today 2017;4(2, Part A):637–44. http://dx.doi.org/10.1016/j.matpr.2017.01.067.

[8] Asiaban R, Khajehsaeid H, Ghobadi E, Jabbari M. New magneto-rheological fluids with high stability: Experimental study and constitutive modelling. Polym Test 2020;106512. http://dx.doi.org/10.1016/j.polymertesting.2020.106512.

[9] Wang F, Ma Y, Zhang H, Gu J, Yin J, Jia X, Zhang H, Wang Y, Fu X, Yu R, Wang Z, Han S, Wang G. Rheological properties and sedimentation stability of magnetorheological fluid based on multi-walled carbon nanotubes/cobalt ferrite nanocomposites. J Molecular Liquids 2021;324:115103. http://dx.doi.org/10.1016/j.molliq.2020.115103.

[10] Zhao X, Kim J, Cezar CA, Huebsch N, Lee K, Bouhadir K, Mooney DJ. Active scaffolds for on-demand drug and cell delivery. Proc Natl Acad Sci USA 2011;108(1):67–72. http://dx.doi.org/10.1073/pnas.1007862108, Epub 2010 Dec 13. PMID: 21149682; PMCID: PMC3017202.

[11] Garcia-Gonzalez D, Landis CM. Magneto-diffusion-viscohyperelasticity for magneto-active hydrogels: rate dependences across time scales. J Mech Phys Solids 2020;139:103934. http://dx.doi.org/10.1016/j.jmps.2020.103934.

[12] Liu X, Liu J, Lin S, Zhao X. Hydrogel machines. Mater Today 2020;36:102–24.

[13] Montgomery SM, Wu S, Kuang X, Armstrong CD, Zemelka C, Ze Q, Zhang R, Zhao R, Qi HJ. Magneto-mechanical metamaterials with widely tunable mechanical properties and acoustic bandgaps. Adv Funct Mater 2021;31(3):2005319. http://dx.doi.org/10.1002/adfm.202005319.

[14] Charles ADM, Rider AN, Brown SA, Wang CH. Multifunctional magneto-polymer matrix composites for electromagnetic interference suppression, sensors and actuators. Progr Mater Sci 2021;115:100705. http://dx.doi.org/10.1016/j.pmatsci.2020.100705.

[15] Kwon SH, Lee CJ, Choi HJ, Chung KH, Jung JH. Viscoelastic and mechanical behaviors of magneto-rheological carbonyl iron/natural rubber composites with magnetic iron oxide nanoparticle. Smart Mater Struct 2019;28(4):045012. http://dx.doi.org/10.1088/1361-665X/ab0018.

[16] Marova LA, Alekhina YA, Rusakova TS, Perov NS. Tunable properties of magnetoactive elastomers for biomedical applications. Phys Proc 2016;82:38–45. http://dx.doi.org/10.1016/j.phpro.2016.05.008.

[17] Xu Y, Gong X, Xuan S, Zhang W, Fan Y. A high-performance magnetorheological material: preparation, characterization and magnetic-mechanic coupling properties. Soft Matter 2011;7(11):5246–54. http://dx.doi.org/10.1039/C1SM05301A.

[18] Bastola AK, Mokarram H. A review on magneto-mechanical characterizations of magnetorheological elastomers. Composites B 2020;108348. http://dx.doi.org/10.1016/j.compositesb.

[19] Cvek M, Kracalik M, Sedlacik M, Mrlik M, Sedlarik V. Reprocessing of injection-molded magnetorheological elastomers based on TPE matrix. Composites B 2019;172:253–61. http://dx.doi.org/10.1016/j.compositesb.2019.05.090.

[20] Hafeez MA, Usman M, Umer MA, Hanif A. Recent progress in isotropic magnetorheological elastomers and their properties: a review. Polymers 2020. http://dx.doi.org/10.3390/polym12123023.

[21] Jung HS, Kwon SH, Choi HJ, Jung JH, Kim YG. Magnetic carbonyl iron/natural rubber composite elastomer and its magnetorheology. Composite Struct 2016;136:106–12. http://dx.doi.org/10.1016/j.compstruct.2015.10.008.

[22] Bastola AK, Paudel M, Li L, Li W. Recent progress of magnetorheological elastomers: a review. Smart Materials and Structures 2020. http://dx.doi.org/10.1088/1361-665X/abbc77.

[23] Garcia-Gonzalez D, Moreno MA, Valencia L, Arias A, Velasco D. Influence of elastomeric matrix and particle volume fraction on the mechanical response of magneto-active polymers. Composites B 2021;215(June):108796. http://dx.doi.org/10.1016/j.compositesb.2021.108796.

[24] Lua AMReyes, Hopf R, Mazza E. Factors influencing the mechanical properties of soft elastomer substrates for traction force microscopy. Mech Soft Mater 2020;2:6. http://dx.doi.org/10.1007/s42558-020-00021-8.

[25] Lee M, Park T, Kim C, Park SM. Characterization of a magneto-active membrane actuator comprising hard magnetic particles with varying crosslinking degrees. Mater Design 2020;195:108921. http://dx.doi.org/10.1016/j.matdes.2020.108921.

[26] Borin D, Stepanov G, Dohmen E. Hybrid magnetoactive elastomer with a soft matrix and mixed powder. Arch Appl Mech 2019;89:105–17. http://dx.doi.org/10.1007/s00419-018-1456-9.

[27] Ivaneyko D, Toshchevikov V, Saphiannikova M, Heinrich G. Effects of particle distribution on mechanical properties of magneto-sensitive elastomers in a homogeneous magnetic field. Condensed Matter Phys 2012. http://dx.doi.org/10.5488/CMP.15.33601.

[28] Garcia-Gonzalez D, Hossain M. A microstructural-based approach to model magneto-viscoelastic materials at finite strains. Int J Solids Struct 2021;208–209:119–32.

[29] Garcia-Gonzalez D, Hossain M. Microstructural modelling of hard-magnetic soft materials: Dipole–dipole interactions versus zeeman effect. Extreme Mech Lett 2021;48:101382. http://dx.doi.org/10.1016/j.eml.2021.101382.

[30] Garcia-Diez A, Rial-Tubio C, Gutierrez-Etxebarria J, Lanceros-Mendez S. Magnetorheological elastomer-based materials and devices: state of the art and future perspectives. Advanced Engineering Materials 2021. http://dx.doi.org/10.1002/adem.202100240.

[31] Koivikko A, Drotlef DM, Sitti M, Sariola V. Magnetically switchable soft suction grippers. Extreme Mech Lett 2021;44:101263.

[32] Zhang J, Ren Z, Hu W, Soon RH, Yasa IC, Liu Z, Sitti M. Voxelated three-dimensional miniature magnetic soft machines via multimaterial heterogeneous assembly. Science Robotics 2021;6:53.

[33] Bastola AK, Li L. A new type of vibration isolator based on magnetorheological elastomer. Mater Design 2018;157:431–6. http://dx.doi.org/10.1016/j.matdes.2018.08.009.

[34] Kallio M, Lindroos T, Aalto S, Järvinen E, Kärnä T, Meinander T. Dynamic compression testing of a tunable spring element consisting of a magnetorheological elastomer. Smart Mater Struct 2007;16(2):506–14. http://dx.doi.org/10.1088/0964-1726/16/2/032.

[35] Sun S, Yang J, Du H, et al. Development of magnetorheological elastomers–based tuned mass damper for building protection from seismic events. J Intell Mater Syst Struct 2018;29(8):1777–89.

[36] Varga Z, Filipcsei G, Zrínyi M. Magnetic field sensitive functional elastomers with tuneable modulus. Polymer 2006;47:227–33.

[37] Zhu M, Fu J, Li W, Xia D, Qi S, Yu M. Design and co-optimization of a laminated isolation bearing based on magnetorheological elastomer. Mechanical Systems and Signal Processing 2021. http://dx.doi.org/10.1016/j.ymssp.2021.107843.

[38] de Souza Eloy F, Gomes GF, Ancelotti AC, da Cunha SS, Bombard AJF, Junqueira DM. A numerical-experimental dynamic analysis of composite sandwich beam with magnetorheological elastomer honeycomb core. Composite Struct 2019;209:242–57. http://dx.doi.org/10.1016/j.compstruct.2018.10.041.

[39] Alkhalaf A, Hooshiar A, Dargahi J. Composite magnetorheological elastomers for tactile displays: Enhanced MR-effect through bi-layer composition. Composites B 2020;190:107888.

[40] Hu T, Xuan S, Ding L, Gong X. Stretchable and magneto-sensitive strain sensor based on silver nanowire-polyurethane sponge enhanced magnetorheological elastomer. Materials & Design 2018. http://dx.doi.org/10.1016/j.matdes.2018.07.024.

[41] Malikan M, Uglov NS, Eremeyev VA. On instabilities and post-buckling of piezomagnetic and flexomagnetic nanostructures. Internat J Engrg Sci 2020;157:103395. http://dx.doi.org/10.1016/j.ijengsci.2020.103395.

[42] Bica I. Influence of the transverse magnetic field intensity upon the electric resistance of the magnetorheological elastomer containing graphite microparticles. Materials Letters 2009. http://dx.doi.org/10.1016/j.matlet.2009.07.032.

[43] Behrooz M, Gordaninejad F. Three-dimensional study of a one-way, flexible magnetorheological elastomer-based micro fluid transport system. Smart Mater Struct 2016;25(9):095012. http://dx.doi.org/10.1088/0964-1726/25/9/095012.

[44] Wu C, Zhang Q, Fan X, Song Y, Zheng Q. Smart magnetorheological elastomer peristaltic pump. J Intell Mater Syst Struct 2019;30(7):1084–93. http://dx.doi.org/10.1177/1045389X19828825.

[45] Kallio M. The elastic and damping properties of magnetorheological elastomers (Dissertation), VTT Technical Research Centre of Finland; 2005, http://www.vtt.fi/inf/pdf/publications/2005/P565.pdf.

[46] Kim Y, Parada GA, Liu S, Zhao X. Ferromagnetic soft continuum robots. Science Robotics 2019;4:33.

[47] Hogan KJ, Mikos AG. Biodegradable thermoresponsive polymers: Applications in drug delivery and tissue engineering. Polymer. 2020;211:123063. http://dx.doi.org/10.1016/j.polymer.2020.123063.

[48] Ren Z, Hu W, Dong X, Sitti M. Multi-functional soft-bodied jellyfish-like swimming. Nature Commun 2019;10:2703.

[49] Hu W, Lum G, Mastrangeli M, et al. Small-scale soft-bodied robot with multimodal locomotion. Nature 2018;554:81–5. http://dx.doi.org/10.1038/nature25443.

[50] Garcia-Gonzalez D, Muñoz Barrutia A. Computational insights into the influence of substrate stiffness on collective cell migration. Extreme Mechanics Lett 2020;40:100928.

[51] Agirre-Olabide I, Berasategui J, Elejabarrieta MJ, Bou-Ali MM. Characterization of the linear viscoelastic region of magnetorheological elastomers. J Intell Mater Syst Struct 2014;25(16):2074–81. http://dx.doi.org/10.1177/1045389X13517310.

[52] Dargahi A, Sedaghati R, Rakheja S. On the properties of magnetorheological elastomers in shear mode: Design, fabrication and characterization. Composites B 2019;159:269–83. http://dx.doi.org/10.1016/j.compositesb.2018.09.080.

[53] Hemmatian M, Sedaghati R, Rakheja S. Characterization and modeling of temperature effect on the shear mode properties of magnetorheological elastomers. Smart Mater Struct 2020;29(11):115001. http://dx.doi.org/10.1088/1361-665X/abb359.

[54] Nam TH, Petríková I, Marvalová B. Experimental characterization and viscoelastic modeling of isotropic and anisotropic magnetorheological elastomers. Polymer Test 2020;81:106272. http://dx.doi.org/10.1016/j.polymertesting.2019.106272.

[55] Atul Narayan SP, Palade LI. Modeling Payne effect with a framework of multiple natural configurations. Intl J Eng Sci 2020;157:103396. http://dx.doi.org/10.1016/j.ijengsci.2020.103396.

[56] Laun HM, Schmidt G, Gabriel C, Kieburg C. Reliable plate–plate MRF magnetorheometry based on validated radial magnetic flux density profile simulations. Rheol Acta 2008;47(9):1049–59. http://dx.doi.org/10.1007/s00397-008-0305-0.

[57] Koo JH, Khan F, Jang DD, Jung HJ. Dynamic characterization and modeling of magneto-rheological elastomers under compressive loadings. Smart Mater Struct 2010;19(11):117002. http://dx.doi.org/10.1088/0964-1726/19/11/117002.

[58] Pelteret JP, Steinmann P. Magneto-active polymers: Fabrication, characterisation, modelling and simulation at the micro- and macro-scale. De Gruyter; 2020, http://dx.doi.org/10.1515/9783110418576.

[59] Khanouki MA Sedaghati R, Hemmatian M. Experimental characterization and microscale modeling of isotropic and anisotropic magnetorheological elastomers. Composites B 2019. http://dx.doi.org/10.1016/j.compositesb.2019.107311.

[60] Vatandoost H, Hemmatian M, Sedaghati R, Rakheja S. Dynamic characterization of isotropic and anisotropic magnetorheological elastomers in the oscillatory squeeze mode superimposed on large static pre-strain. Composites B 2020. http://dx.doi.org/10.1016/j.compositesb.2019.107648.

[61] Brask JB, Singla-Buxarrais G, Uroz M, Vincent R, Trepat X. Compressed sensing traction force microscopy. Acta Biomater 2015. http://dx.doi.org/10.1016/j.actbio.2015.08.023.

[62] Lokander M, Stenberg B. Performance of isotropic magnetorheological rubber materials. Polym Test 2003;22(3):245–51. http://dx.doi.org/10.1016/S0142-9418(02)00043-0.

[63] Morillas JR, de Vicente J. Magnetorheology: a review. Soft Matter 2020. http://dx.doi.org/10.1039/D0SM01082K.

[64] Meyvis TKL, Stubbe BG, Steenbergen MJV, Hennink WE, Smedt SCD, Demeester J. A comparison between the use of dynamic mechanical analysis and oscillatory shear rheometry for the characterisation of hydrogels. Int J Pharm 2002.

[65] Siviour CR, Walley SM. Inertial and frictional effects in dynamic compression testing. In: The Kolsky-Hopkinson bar machine. Cham: Springer International Publishing; 2018, p. 205–47. http://dx.doi.org/10.1007/978-3-319-71919-1_8.

[66] Bustamante R, Shariff MHBM, Hossain M. Mathematical formulations for elastic magneto-electrically coupled soft materials at finite strains: Time-independent processes. Internat J Engrg Sci 2021;159:103429.

[67] Cantera MA, Behrooz M, Gibson RF, Gordaninejad F. Modeling of magneto-mechanical response of magnetorheological elastomers (mre) and mre-based systems: a review. Smart Materials and Structures 2017. http://dx.doi.org/10.1088/1361-665X/aa549c.

[68] Gao W, Wang X. Experimental and theoretical investigations on magnetoelastic shear behavior of isotropic MR elastomers under gradient magnetic fields. J Magn Magn Mater 2019;483:196–204.

[69] Qiao Y, Zhang J, Zhang M, Liu L, Zhai P. A magnetic field- and frequency-dependent dynamic shear modulus model for isotropic silicone rubber-based magnetorheological elastomers. Compos Sci Technol 2021;204. http://dx.doi.org/10.1016/j.compscitech.2020.108637.

[70] Keip MA, Sridhar A. A variationally consistent phase-field approach for micro-magnetic domain evolution at finite deformations. J Mech Phys Solids 2019;125:805–24.

[71] Mukherjee D, Bodelot L, Danas K. Microstructurally-guided explicit continuum models for isotropic magnetorheological elastomers with iron particles. Int J Non-Linear Mech 2020;120:103380.

[72] Danas K, Kankanala SV, Triantafyllidis N. Experiments and modeling of iron-particle-filled magnetorheological elastomers. J Mech Phys Solids 2012;60(1):120–38. http://dx.doi.org/10.1016/J.JMPS.2011.09.006.

[73] Gaunt P. Magnetic viscosity and thermal activation energy. J Appl Phys 1986;59(12):4129–32. http://dx.doi.org/10.1063/1.336671.

[74] Kreissl P, Holm C, Weeber R. Frequency-dependent magnetic susceptibility of magnetic nanoparticles in a polymer solution: a simulation study. Soft Matter 2021;17(1):174–83. http://dx.doi.org/10.1039/D0SM01554G.

[75] Lyberatos A. Magnetic viscosity and the field rate dependence of the magnetization. J Magn Magn Mater 1999;202(1):239–50. http://dx.doi.org/10.1016/S0304-8853(99)00305-4.

[76] Wohlfarth EP. The coefficient of magnetic viscosity. J Phys F 1984;14(8):L155–9. http://dx.doi.org/10.1088/0305-4608/14/8/005.

[77] Chantrell RW, Lyberatos A, Wohlfarth PE. The coefficient of magnetic viscosity. II. The time dependence of the magnetisation of interacting fine-particle magnetic materials. J Phys F. http://dx.doi.org/10.1088/0305-4608/16/7/006.

[78] Walter BL, Pelteret JP, Steinmann PKaschtaJSchubertDW. On the wall slip phenomenon of elastomers in oscillatory shear measurements using parallel-plate rotational rheometry: I. Detecting wall slip. Polym Test. http://dx.doi.org/10.1016/j.polymertesting.2017.05.035.

[79] Walter BL, Pelteret JP, J. Kaschta, Schubert DW, Steinmann P. Preparation of magnetorheological elastomers and their slip-free characterization by means of parallel-plate rotational rheometry. Smart Mater Struct. http://dx.doi.org/10.1088/1361-665X/aa6b63.

[80] Bica I, Anitas EM, Averis LME, Kwon SH, Choi HJ. Magnetostrictive and viscoelastic characteristics of polyurethane-based magnetorheological elastomer. J Ind Eng Chem 2019;73:128–33. http://dx.doi.org/10.1016/j.jiec.2019.01.015.

[81] Kankanala SV, Triantafyllidis N. On finitely strained magnetorheological elastomers. J Mech Phys Solids 2004;52(12):2869–908. http://dx.doi.org/10.1016/j.jmps.2004.04.007.

[82] Romeis D, Toshchevikov V, Saphiannikova M. Effects of local rearrangement of mag- netic particles on deformation in magneto-sensitive elastomers. Soft Matter 2019;15(17):3552–64. http://dx.doi.org/10.1039/C9SM00226J.

[83] Wu H, Xu Z, Wang J, Bo X, Tang Z, Jiang S, Zhang G. Chain formation mechanism of magnetic particles in magnetorheological elastomers during pre-structure. J Magn Magn Mater 2021;527:167693.
[84] Vatandoost H, Sedaghati R, Rakheja S, Hemmatian M. Effect of pre-strain on compression mode properties of magnetorheological elastomers. Polymer Test 2021;93. http://dx.doi.org/10.1016/j.polymertesting.2020.106888.
[85] Liao G, Gong X, Xuan S, Guo C, Zong L. Magnetic-field-induced normal force of magnetorheological elastomer under compression status. Ind Eng Chem Res 2012;51(8):3322–8. http://dx.doi.org/10.1021/ie201976e.
[86] Adebowale K, Gong Z, Hou JC, et al. Enhanced substrate stress relaxation promotes filopodia-mediated cell migration. Nat Mater 2021. http://dx.doi.org/10.1038/s41563-021-00981-w.